W H Matthaeus
University of Delaware

Heliospheric physical processes for understanding
Solar-Terrestrial Relations
September 21-26, 2015 - L'Aquila, Italy

More detailed cascade picture: central role of
higher order correlations/higher order statistics

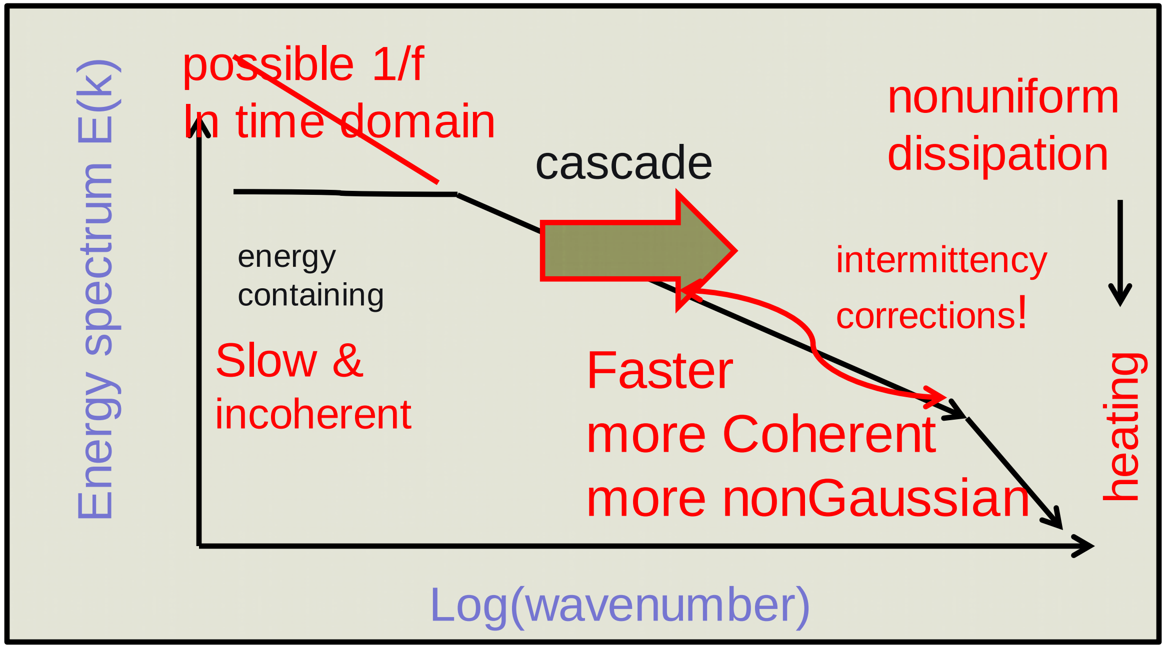

- **Cascade:** *progressively enhances nonGaussian character*
- *Generation of* ***coherent structures*** *and patchy correlations*
- *Coherent structures are sites of* ***enhanced dissipation***
- for inverse cascade/quasi-invariant case, **1/f noise** low frequency irregularity in time, and build up of long wavelegnth fluctuations

VanDyke, An Album of Fluid Motion

Mean flow and fluctuations

- In turbulence there can be great differences between mean state and fluctuating state
- Example: Flow around sphere at R = 15,000

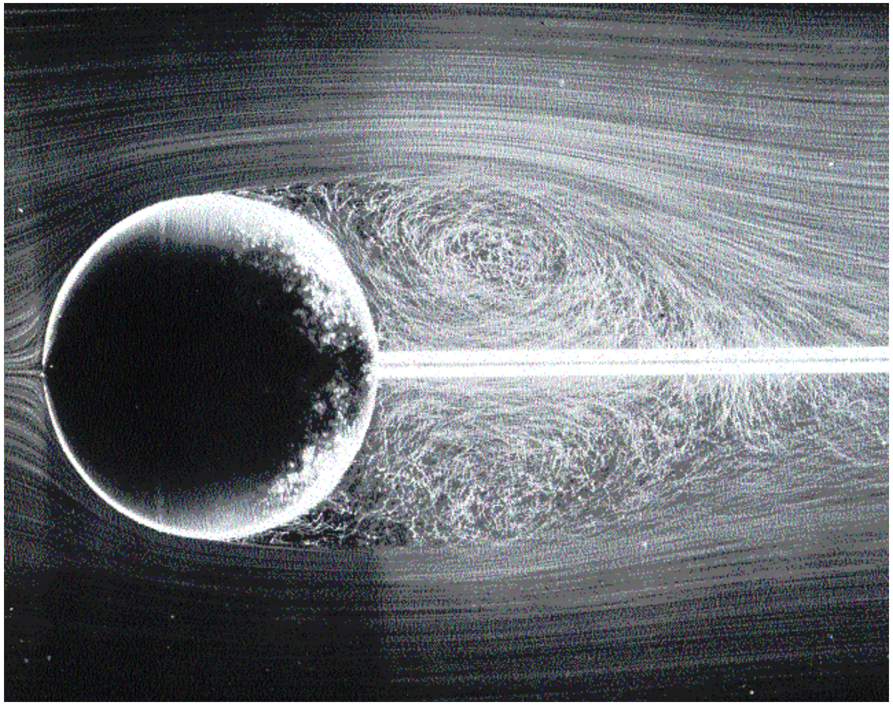

Mean flow

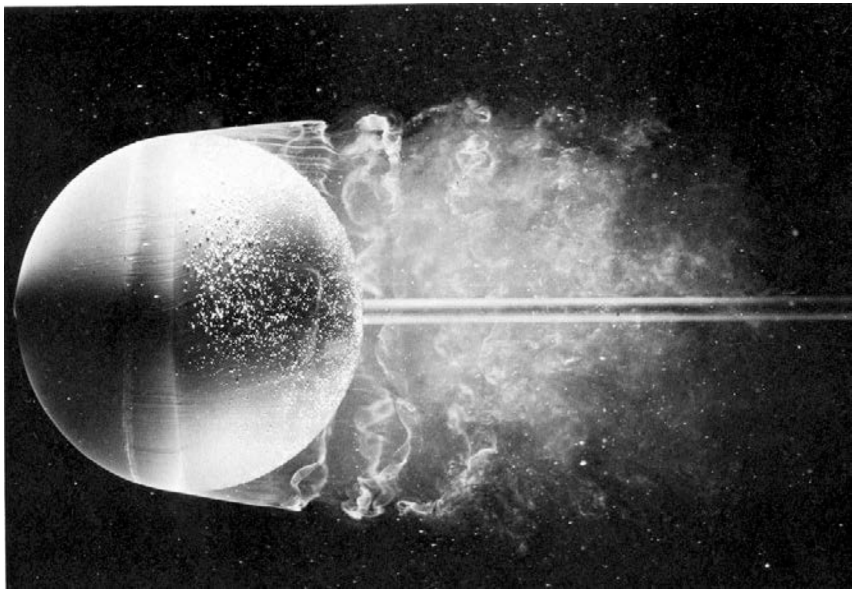

Instantaneous flow

Visualizing Solar wind turbulence !

Using heliospheric imagers (e.g., Stereo) and recent developments in image processing permits us to see solar wind, CMEs and solar wind turbulence

Courtesy of Craig Deforest.

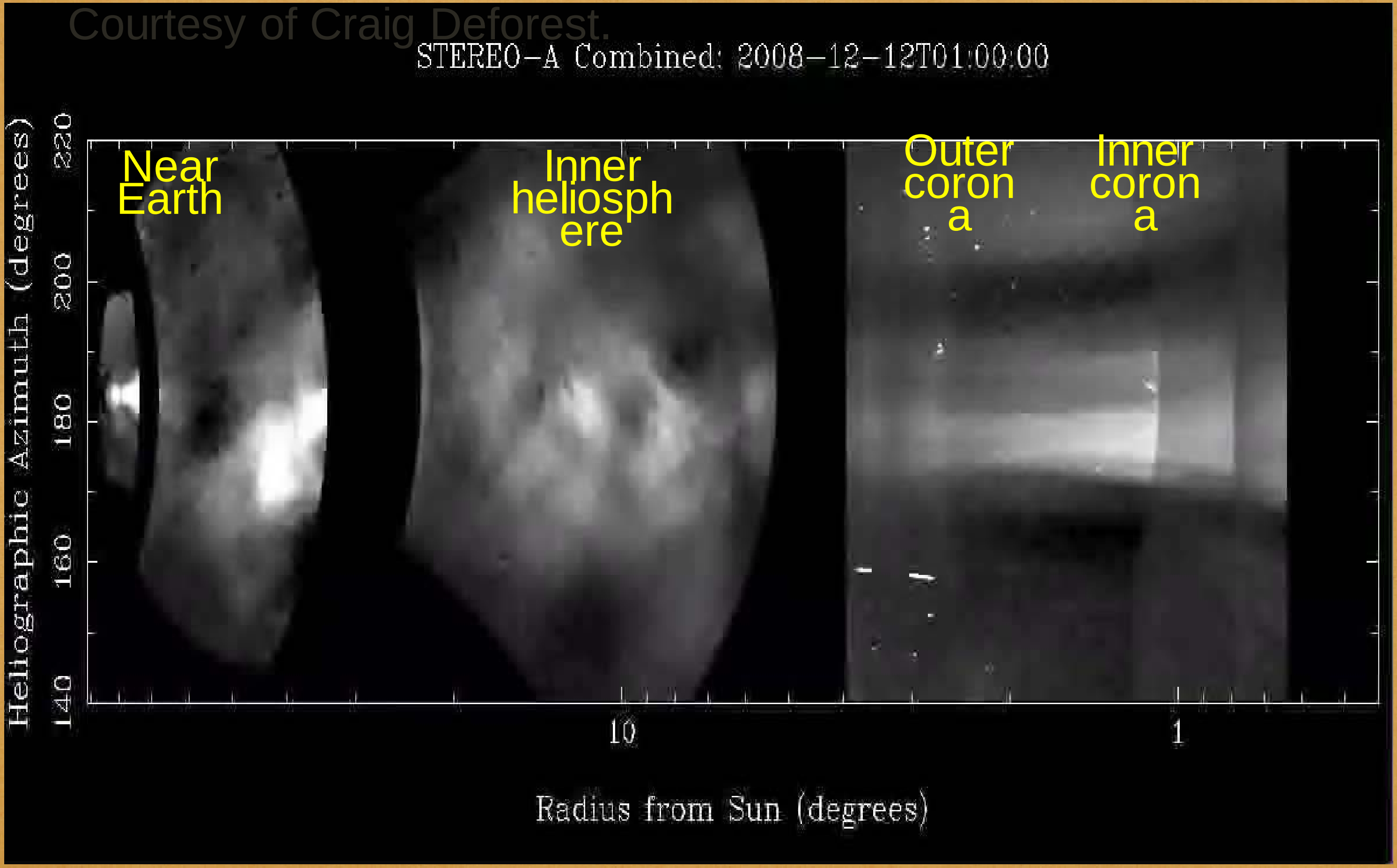

Large scales, turbulence and kinetic scales

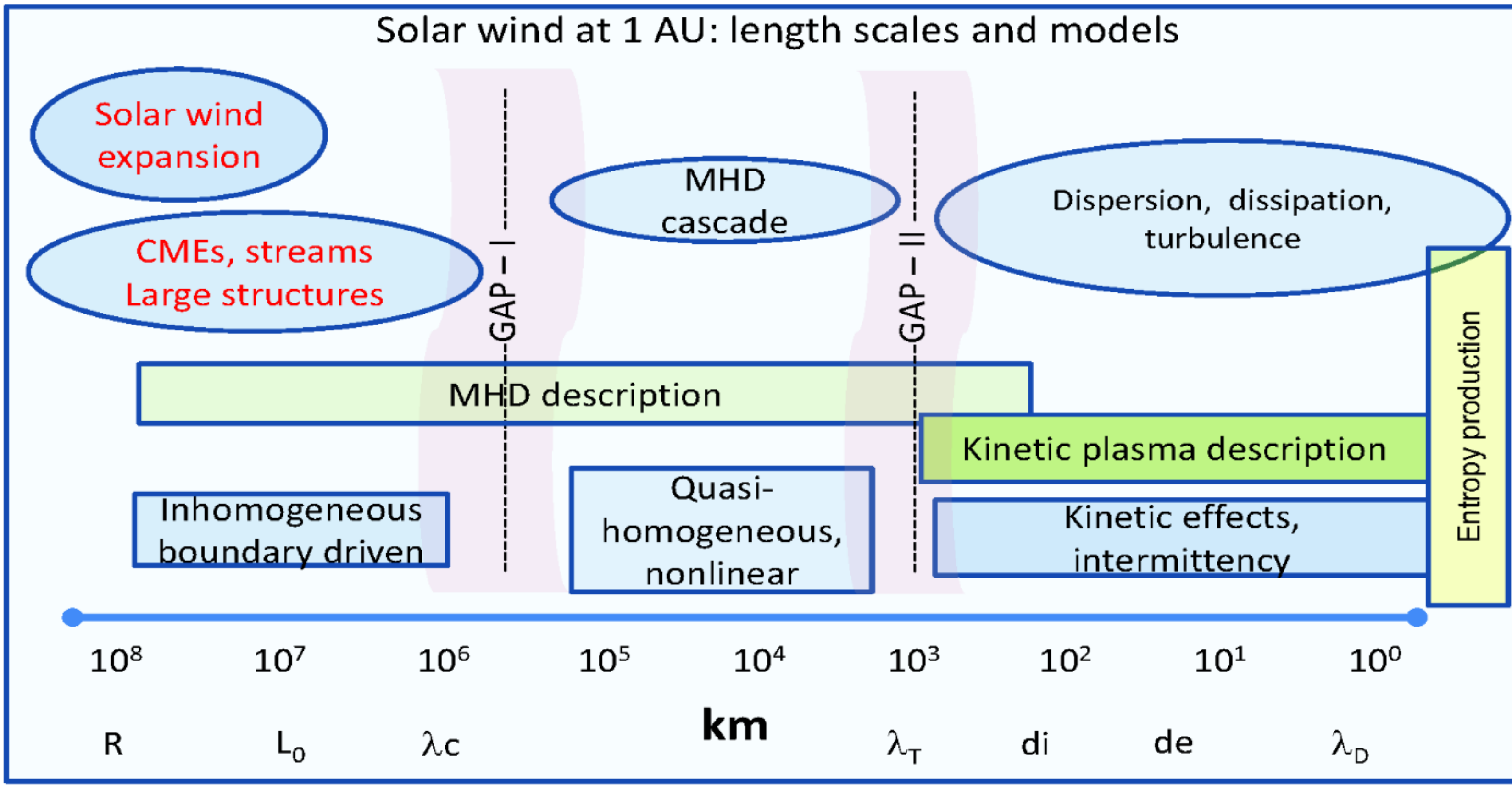

Unresolved turbulence is modeled dynamically

Coronal/interplanetary dynamical models (MHD) with turbulence modeling

- Single fluid
- Isothermal or polytropic with $\gamma \rightarrow 1$
- Ad hoc heat function
- no cross helicity effect
- WKB waves
- strong heat conduction (acing on all species)

Partial list of advances

- Heinemann& Olbert JGR (1980)
- Tu et al JGR (1984); Tu JGR (1988)
- Hollweg, JGR, 1986; Hollweg & Johnson (1988
- Velli et al. GAFD (1991); Velli AA (1993)
- Matthaeus et al JGR (1994); Zank et al JGR (1996);;

  Matthaeus et al, PRL(1999); Smith et al JGR (2000):

  Breech et al, JGR (2008); Isenberg et al ApJ (2010);

  Zank et al ApJ (2012)
- Verdini et al, SOHO-2006; ApJL, 2010
- Cranmer et al, ApJS 2007
- Lionello et al 2014)
- Usmanov et al JGR (2000)
- Usmanov et al, 2008, 2010, ApJ 2011, 2012

  Usmanov et al, 2013; Usmamov et al ApJ (2014

,

- nonWKB transport of fluctuations
- Cross helicity effect
- vonKarman-MHD heating - proton fluid,
- Separate proton/multifliuid enegy equations
- no heat conduction on protons
- physical modeling of the Reynolds stresses

- Consistent modeling of production/mixing terms
- Polytropic γ =5/3 EOS
- Strong heat conduction on electrons only
- no ad hoc heat function
- Optimized von Karman MHD dissipation
- Analytical improvements in transport modeling
- Improved understanding of nonconserved quantities (e.g., residual energy)

SOON! →

- Proper turbulence modeling of Reynolds stresses
- Improved turbulence production by mean (large scale) fields
- Eddy viscosity (velocity & magnetic; alpha effect; turbulent resistivity, turbulent heat conduction
- More complete multifluid p/e models
- Turbulence modeling with tuned energy and length equations
- p/e/ion Heat functions based on kinetic plasma physcs

Self consistent large scale simulation with turbulence modeling

Usmanov et al, ApJ 788 43 2014

- **3D MHD large scale modeling** in rotating frame (Reynolds averaged)
- **Reynolds averaging** implies new dynamical terms
  - PONDEROMOTIVE FORCE(WAVE PRESSURE)
  - DIV (Reynolds stresses)
    - "mixing terms" & energy difference
    - Turbulent viscosity
    - Turbulent resistivity
  - TURB. INDUCED ELECTRIC FIELD (alpha effect)
  - HEAT FUNCTIONS (ion & electron internal energies)
  - PRESSURE EFFECTS (convective and compressional)
    - Turbulent heat conduction
- **Turbulence transport model**
  - Fluctuation energy
  - Cross helicity
  - Correlation scale(s)
  - vonKarman-Howarth heating $\sim Z^3/L$

- Response of **kinetic scale plasma turbulence**
  - Phenomenology under development
  - Intermittency of dissipation (like hydro & MHD)
  - Partitioning of dissipated energy among species (protons, electrons, ions, suprathermals…)

Reynolds averaged equations

- Mass
- Momentum
- Magnetic induction
- Proton pressure
- Pickup ion pressure
- Electron pressure

$$\frac{\partial N_S}{\partial t} + \nabla \cdot (N_S \mathbf{v}) = -\, q_{\mathrm{ex1}}, \tag{8}$$

$$\begin{aligned}
&\frac{\partial (\rho \mathbf{v})}{\partial t} + \nabla \cdot \Big[\rho \mathbf{v}\mathbf{v} - \frac{1}{4\pi}\mathbf{B}\mathbf{B} \\
&\quad + \Big(P_S + P_E + P_I + \underline{\frac{\langle B'^2 \rangle}{8\pi}} + \frac{B^2}{8\pi} \Big)\mathbf{I} + \underline{\mathcal{R}} \Big] \\
&\quad + \rho \left[\frac{GM_\odot}{r^2}\hat{\mathbf{r}} + 2\boldsymbol{\Omega} \times \mathbf{v} + \boldsymbol{\Omega} \times (\boldsymbol{\Omega} \times \mathbf{r}) \right] \\
&= -\, m_p [(q_{\mathrm{ex1}} + q_{\mathrm{ex2}})\mathbf{u} + q_{\mathrm{ph}}\, \boldsymbol{\Omega} \times \mathbf{r}],
\end{aligned} \tag{9}$$

$$\frac{\partial \mathbf{B}}{\partial t} = \nabla \times (\mathbf{v} \times \mathbf{B} + \underline{\sqrt{4\pi\rho}\, \boldsymbol{\varepsilon}_m}), \tag{10}$$

$$\begin{aligned}
&\frac{\partial P_S}{\partial t} + (\mathbf{v} \cdot \nabla) P_S + \gamma P_S \nabla \cdot \mathbf{v} + \frac{\gamma P_S}{N_S} q_{\mathrm{ex1}} + (\gamma - 1)\frac{P_S - P_E}{\tau_{\mathrm{SE}}} \\
&\quad + \underline{\langle (\mathbf{v}' \cdot \nabla) P_S' \rangle} + \underline{\gamma \langle P_S' \nabla \cdot \mathbf{v}' \rangle} = \underline{f_p Q_1(\mathbf{r})},
\end{aligned} \tag{11}$$

$$\frac{\partial N_I}{\partial t} + \nabla \cdot (N_I \mathbf{v}) = q_{\mathrm{ex1}} + q_{\mathrm{ph}}, \tag{12}$$

$$\begin{aligned}
&\frac{\partial P_I}{\partial t} + (\mathbf{v} \cdot \nabla) P_I + \frac{5}{3} P_I \nabla \cdot \mathbf{v} + \underline{\langle (\mathbf{v}' \cdot \nabla) P_I' \rangle} + \underline{\tfrac{5}{3} \langle P_I' \nabla \cdot \mathbf{v}' \rangle} \\
&= (q_{\mathrm{ex1}} + q_{\mathrm{ph}}) \frac{m_p (u^2 + \underline{\langle v'^2 \rangle})}{3} - \underline{Q_2(\mathbf{r})},
\end{aligned} \tag{13}$$

$$\begin{aligned}
&\frac{\partial P_E}{\partial t} + (\mathbf{v} \cdot \nabla) P_E + \gamma P_E \nabla \cdot \mathbf{v} - \frac{\gamma P_E}{N_E} q_{\mathrm{ph}} + (\gamma - 1) \\
&\quad \times \left[\frac{P_E - P_S}{\tau_{\mathrm{SE}}} + \nabla \cdot \mathbf{q}_H \right] \\
&\quad + \underline{\langle (\mathbf{v}' \cdot \nabla) P_E' \rangle} + \gamma \underline{\langle P_E' \nabla \cdot \mathbf{v}' \rangle} = \underline{(1 - f_p) Q_1(\mathbf{r})},
\end{aligned} \tag{14}$$

Eddy viscosity approximation (Boussinesq, Smagorinsky, Yoshizawa, Yokoi…)

$$\boldsymbol{\mathcal{R}} = \langle \rho \mathbf{v}'\mathbf{v}' - \mathbf{B}'\mathbf{B}'/4\pi \rangle$$

$$\frac{1}{\rho}\boldsymbol{\mathcal{R}} = \frac{2}{3}K_R\,\mathbf{I} - \nu_K \boldsymbol{\mathcal{S}} + \nu_M \boldsymbol{\mathcal{M}}$$

where ν_K and ν_M are (kinematic) eddy viscosity coefficients, $K_R = \langle v'^2 - b'^2\rangle/2 = \sigma_D Z^2/2$ is the residual energy, and $\boldsymbol{\mathcal{S}}$ and $\boldsymbol{\mathcal{M}}$ are the strain rates of the mean velocity $\mathbf{u}$ and the mean Alfvén velocity $\mathbf{V}_A = \mathbf{B}(4\pi\rho)^{-1/2}$, respectively. $\boldsymbol{\mathcal{S}}$ and $\boldsymbol{\mathcal{M}}$ are deviatoric (traceless) symmetric tensors given by

$$\boldsymbol{\mathcal{S}} = \nabla\mathbf{u} + \nabla\mathbf{u}^T - \frac{2}{3}(\nabla\cdot\mathbf{u})\mathbf{I}, \qquad \boldsymbol{\mathcal{M}} = \nabla\mathbf{V}_A + \nabla\mathbf{V}_A^T - \frac{2}{3}(\nabla\cdot\mathbf{V}_A)\mathbf{I},$$

$$\boldsymbol{\varepsilon}_m = \langle \mathbf{v}' \times \mathbf{B}' \rangle (4\pi\rho)^{-1/2}$$

$$\boldsymbol{\varepsilon}_m = \bar{\alpha}\mathbf{B} - \bar{\beta}\nabla \times \mathbf{V}_A + \bar{\gamma}\nabla \times \mathbf{v}.$$

α dynamo parameter → magnetic helicity

β beta effect; turbulent resistivity

γ emf due to vorticity

Three equation turbulence transport model closes the system at the MHD level

- Turbulence energy
- Cross helicity
- Correlation scale

$$\frac{\partial Z^2}{\partial t} = -(\mathbf{v}\cdot\nabla)Z^2 - \frac{2}{\rho}\boldsymbol{\mathcal{R}}:\nabla\mathbf{u} + \frac{Z^2(\sigma_D - 1)}{2}\nabla\cdot\mathbf{u} - \frac{\alpha f^+(\sigma_c)Z^3}{\lambda},$$

$$\frac{\partial (Z^2\sigma_c)}{\partial t} = -(\mathbf{v}\cdot\nabla)(Z^2\sigma_c) - 2\varepsilon_m\cdot(\nabla\times\mathbf{u}) - \frac{Z^2\sigma_c}{2}\nabla\cdot\mathbf{u} - \frac{\alpha f^-(\sigma_c)Z^3}{\lambda},$$

$$\frac{\partial \lambda}{\partial t} = -(\mathbf{v}\cdot\nabla)\lambda + \beta f^+(\sigma_c)Z.$$

→ Eddy viscosity, turbulent resistivity, alpha effect, beta and gamma coefficients are determined by Z, λ and σc.

→ All transport coefficients are ~Zλ with O(1) constants determined by other theories or phenomenologies

For brevity terms involving large scale magnetic field & V_A are omitted here, but retained in the coronal model; These are small in the outer heliosphere

Heating due to cascade

- Heating rate (von Karman) is

$$Q_1 = (\gamma - 1)\alpha\, f^+(\sigma_c)\frac{Z^3}{\lambda}$$

with α constant O(1)

$$f^{\pm}(\sigma_c) = (1-\sigma_c^2)^{1/2}[(1+\sigma_c)^{1/2} \pm (1-\sigma_c)^{1/2}]/2$$

The internal energy equations have heat functions

$f_p Q_1$ for protons

$(1 - fp)\, Q_1$ for electrons

The selection of a value for f_p depends entirely on kinetic plasma physics

Large scale (global) model with turbulence modeling

A. Usmanov, M. Goldstein,
B. W. Matthaeus (2014)

Large scale (mean field) model equations:
- Momentum
- Magnetic field
- Density
- internal energies (Te & Tp)
- additional species (Pis, alphas, etc)

NEW TERMS:
- Fluctuation pressure
- Reynolds stresses
- Random compressions
- Turbulent electric field
- Turbulent heat conduction
- Heat function/dissipation

Closures:
- **Eddy viscosity (kinetic & magnetic)**
- **Production/mixing terms**
- **Turbulent transport coefficients**

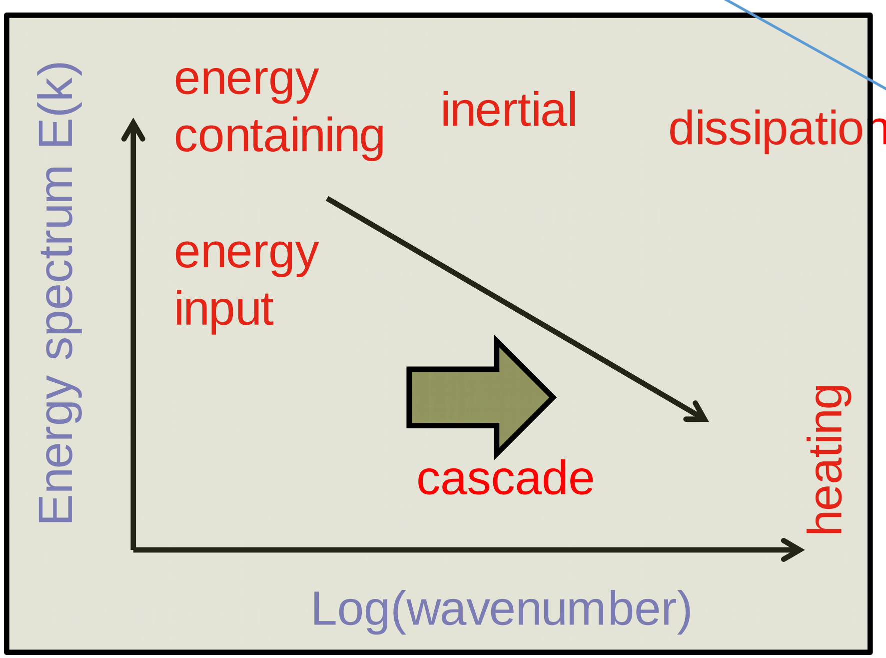

turbulence parameters:
Transport equations for energy, cross helicity, correlation scales

Plasma kinetic theory:
- branching between e/p heating
- Dissipation mechanisms

Usmanov et al model

$$\frac{\partial N_S}{\partial t} + \nabla \cdot (N_S \mathbf{v}) = -q_{\mathrm{ex1}}, \qquad (8)$$

$$\frac{\partial(\rho\mathbf{v})}{\partial t} + \nabla \cdot \left[\rho\mathbf{v}\mathbf{v} - \frac{1}{4\pi}\mathbf{B}\mathbf{B} + \left(P_S + P_E + P_I + \underline{\frac{\langle B'^2\rangle}{8\pi}} + \frac{B^2}{8\pi}\right)\mathbf{I} + \underline{\mathcal{R}}\right]$$
$$+ \rho\left[\frac{GM_\odot}{r^2}\hat{\mathbf{r}} + 2\mathbf{\Omega}\times\mathbf{v} + \mathbf{\Omega}\times(\mathbf{\Omega}\times\mathbf{r})\right] = -m_p[(q_{\mathrm{ex1}} + q_{\mathrm{ex2}})\mathbf{u} + q_{\mathrm{ph}}\,\mathbf{\Omega}\times\mathbf{r}], \qquad (9)$$

$$\frac{\partial \mathbf{B}}{\partial t} = \nabla \times (\mathbf{v}\times\mathbf{B} + \underline{\sqrt{4\pi\rho}\,\boldsymbol{\varepsilon}_m}), \qquad (10)$$

$$\frac{\partial P_S}{\partial t} + (\mathbf{v}\cdot\nabla)P_S + \gamma P_S \nabla\cdot\mathbf{v} + \frac{\gamma P_S}{N_S}q_{\mathrm{ex1}} + (\gamma-1)\frac{P_S - P_E}{\tau_{\mathrm{SE}}}$$
$$+ \underline{\langle(\mathbf{v}'\cdot\nabla)P_S'\rangle} + \gamma\underline{\langle P_S'\nabla\cdot\mathbf{v}'\rangle} = \underline{f_p Q_1(\mathbf{r})}, \qquad (11)$$

$$\frac{\partial N_I}{\partial t} + \nabla\cdot(N_I\mathbf{v}) = q_{\mathrm{ex1}} + q_{\mathrm{ph}}, \qquad (12)$$

$$\frac{\partial P_I}{\partial t} + (\mathbf{v}\cdot\nabla)P_I + \frac{5}{3}P_I\nabla\cdot\mathbf{v} + \underline{\langle(\mathbf{v}'\cdot\nabla)P_I'\rangle} + \underline{\tfrac{5}{3}\langle P_I'\nabla\cdot\mathbf{v}'\rangle}$$
$$= (q_{\mathrm{ex1}} + q_{\mathrm{ph}})\frac{m_p(u^2 + \underline{\langle v'^2\rangle})}{3} - \underline{Q_2(\mathbf{r})}, \qquad (13)$$

$$\frac{\partial P_E}{\partial t} + (\mathbf{v}\cdot\nabla)P_E + \gamma P_E\nabla\cdot\mathbf{v} - \frac{\gamma P_E}{N_E}q_{\mathrm{ph}} + (\gamma-1)\times\left[\frac{P_E - P_S}{\tau_{\mathrm{SE}}} + \nabla\cdot\mathbf{q}_H\right]$$
$$+ \underline{\langle(\mathbf{v}'\cdot\nabla)P_E'\rangle} + \gamma\underline{\langle P_E'\nabla\cdot\mathbf{v}'\rangle} = \underline{(1-f_p)Q_1(\mathbf{r})}, \qquad (14)$$

$$\mathcal{R} = \langle\rho\mathbf{v}'\mathbf{v}' - \mathbf{B}'\mathbf{B}'/4\pi\rangle$$

$$\frac{1}{\rho}\mathcal{R} = \frac{2}{3}K_R\mathbf{I} - \nu_K\mathcal{S} + \nu_M\mathcal{M}$$

where ν_K and ν_M are (kinematic) eddy viscosity coefficients, $K_R = \langle v'^2 - b'^2\rangle/2 = \sigma_D Z^2/2$ is the residual energy, and $\mathcal{S}$ and $\mathcal{M}$ are the strain rates of the mean velocity $\mathbf{u}$ and the mean Alfvén velocity $\mathbf{V}_A = \mathbf{B}(4\pi\rho)^{-1/2}$, respectively. $\mathcal{S}$ and $\mathcal{M}$ are deviatoric (traceless) symmetric tensors given by

$$\mathcal{S} = \nabla\mathbf{u} + \nabla\mathbf{u}^T - \frac{2}{3}(\nabla\cdot\mathbf{u})\mathbf{I}, \quad \mathcal{M} = \nabla\mathbf{V}_A + \nabla\mathbf{V}_A^T - \frac{2}{3}(\nabla\cdot\mathbf{V}_A)\mathbf{I},$$

$$\boldsymbol{\varepsilon}_m = \langle\mathbf{v}'\times\mathbf{B}'\rangle(4\pi\rho)^{-1/2}$$

$$\boldsymbol{\varepsilon}_m = \bar{\alpha}\mathbf{B} - \bar{\beta}\nabla\times\mathbf{V}_A + \bar{\gamma}\nabla\times\mathbf{v}.$$

→ Eddy viscosity, turbulent resistivity, alpha effect, beta and gamma coefficients are determined by Z, λ and σc.

→ All transport coefficients are ~Zλ with O(1) constants determined by other theories or phenomenologies

→ Random compressions and turbulent heat transport are included in the formalism but not yet modeled.

$$\frac{\partial Z^2}{\partial t} = -(\mathbf{v}\cdot\nabla)Z^2 - \frac{2}{\rho}\mathcal{R}:\nabla\mathbf{u} + \frac{Z^2(\sigma_D - 1)}{2}\nabla\cdot\mathbf{u} - \frac{\alpha f^+(\sigma_c)Z^3}{\lambda},$$

$$\frac{\partial(Z^2\sigma_c)}{\partial t} = -(\mathbf{v}\cdot\nabla)(Z^2\sigma_c) - 2\boldsymbol{\varepsilon}_m\cdot(\nabla\times\mathbf{u}) - \frac{Z^2\sigma_c}{2}\nabla\cdot\mathbf{u} - \frac{\alpha f^-(\sigma_c)Z^3}{\lambda},$$

$$\frac{\partial\lambda}{\partial t} = -(\mathbf{v}\cdot\nabla)\lambda + \beta f^+(\sigma_c)Z.$$

$$f^\pm(\sigma_c) = (1-\sigma_c^2)^{1/2}[(1+\sigma_c)^{1/2} \pm (1-\sigma_c)^{1/2}]/2$$

- Heating rate (von Karman) is

$$Q_1 = (\gamma - 1)\alpha f^+(\sigma_c)\frac{Z^3}{\lambda}$$

with α constant O(1)

The internal energy equations have heat functions

fpQ_1 for protons

$(1 - fp)\,Q_1$ for electrons

The selection of a value for f_p depends entirely on kinetic plasma physics

For turbulence transport terms at order Va, see Matthaeus et al, JGR, 1994; Zank et al, ApJ, 2012)

Testing global turbulence transport models

- Need boundary data and constraints from observations
- "causality limit" works in our favor
- Improved modeling approaches
- 1 AU data is *always* important!

Large objects in the SW, an expanding flow (> a few degrees viewed from sun) mainly move along characteristics relatively unaffected by turbulent mixing and field line random walk

Using 1 AU speed and Tp data to refine turbulence transport calculations out to Voyager position and time

Data: symbols

Transport: line

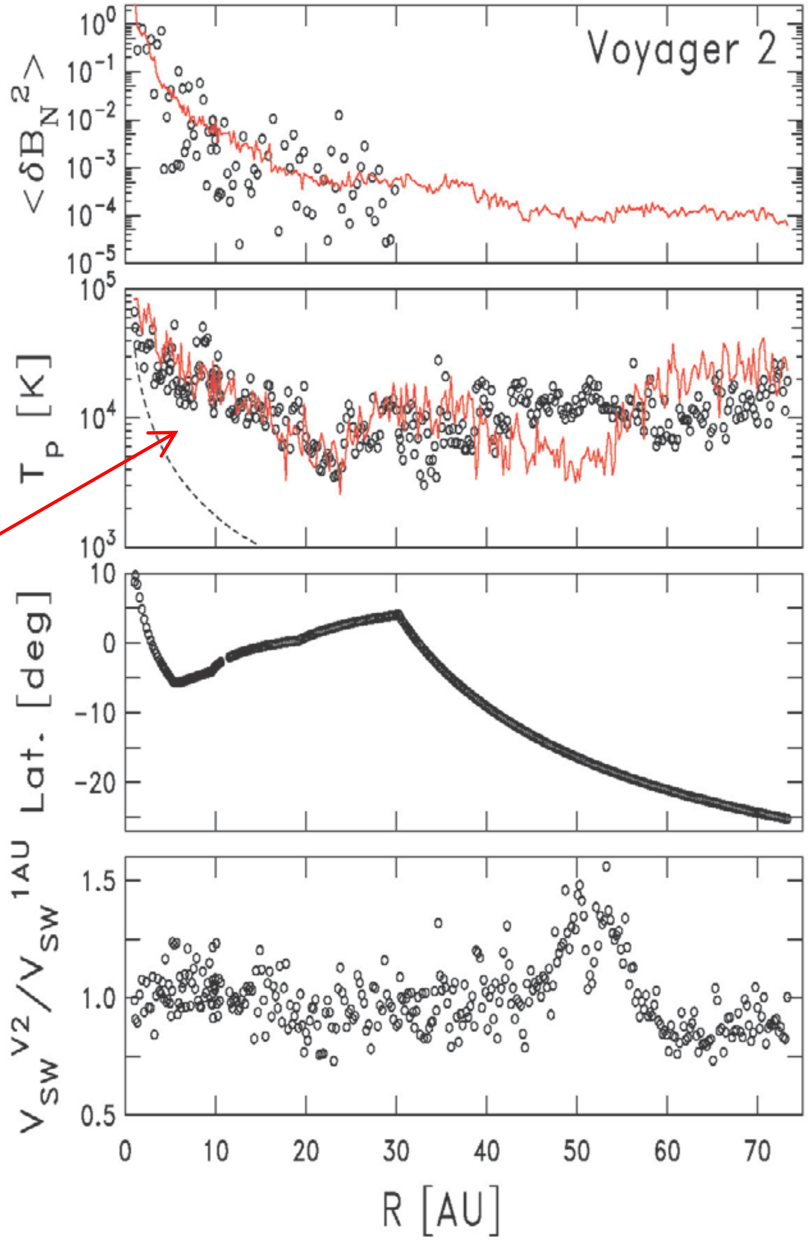

Smith et al, JGR, 2006

Fig. 3.—Results of *Voyager 2* data analysis and predictions of theory using the 1 AU Omnitape observations as input. Black circles represent the observed quantities, and the red solid line shows the theoretical prediction. The IMF fluctuation energy (*top*), proton temperature (*second from top*), spacecraft latitude (*third from top*), and ratio of wind speed at *Voyager* to the observed wind speed within the Omnitape (*bottom*) are shown. The proton temperature predicted from adiabatic expansion from 1 AU is shown as a dashed line on the T_p panel.

Turbulence transport models (in various forms) work pretty well

EG: Here, supplemented by empirical Tp-speed relation at 1 AU, transport model does a pretty good job accounting for Voyager Tp out to 50 AU

Richardson & Smith, GRL, 2003

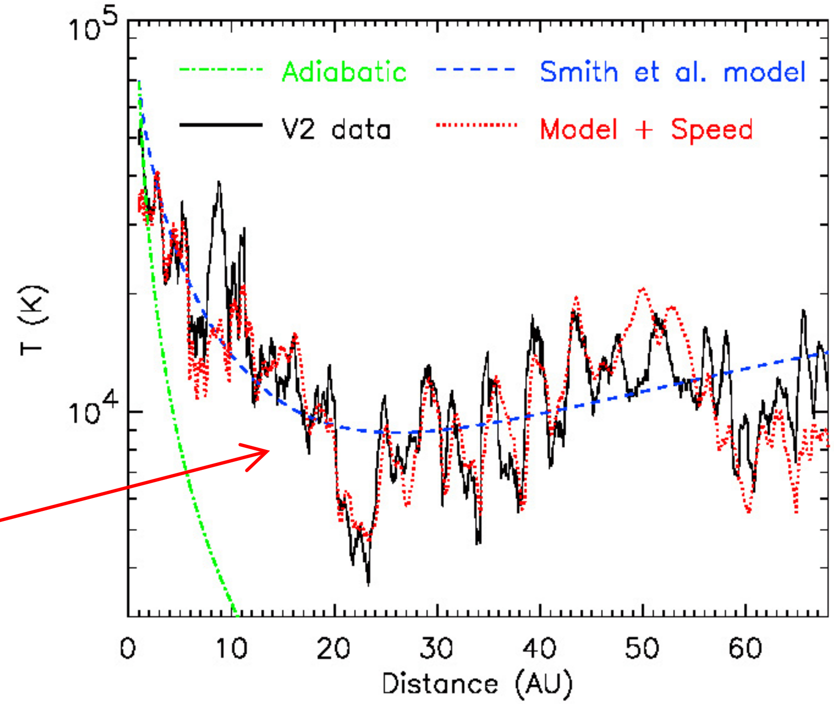

Figure 1. 101-day running boxcar averages of the Voyager 2 temperature (solid line) versus radial distance, the adiabatic profile (dot-dash line), the *Smith et al.* [2001] model result (dashed line), and a superposition of the *Smith et al.* [2001] model and a speed-temperature relation (dotted line).

Global
simulation
Including
transport
& turbulence
modeling:

No dipole tilt

Usmanov et al, ApJ, 2014

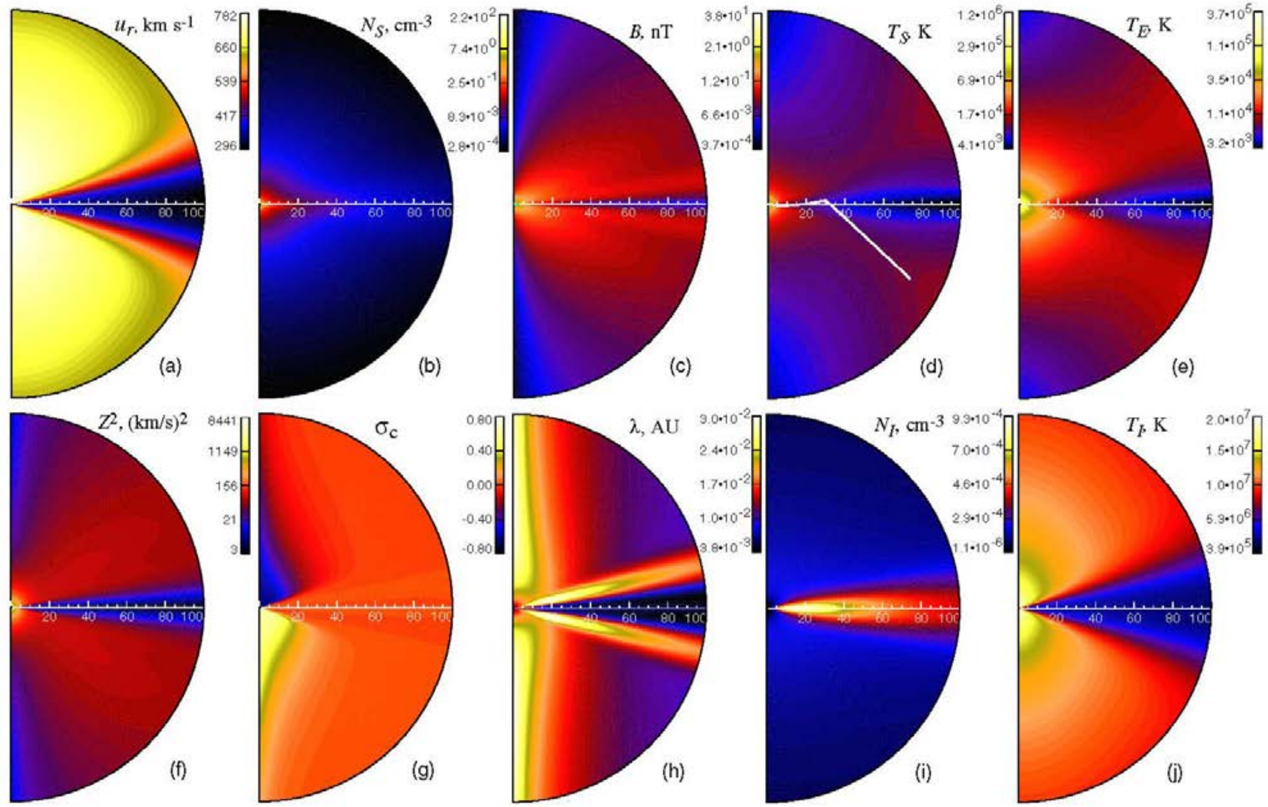

Figure 2. Contour plots of the computed parameters in the meridional plane from 0.3 to 100 AU for the axisymmetric case of a magnetic dipole on the Sun aligned with the solar rotation axis: (a) the radial velocity u_r, (b) the number density of solar wind protons N_S, (c) the magnetic field magnitude B, (d) the temperature of solar wind protons T_S, (e) the temperature of electrons T_E, (f) the turbulence energy Z^2, (g) the normalized cross helicity σ_c, (h) the correlation length scale λ, (i) the number density N_I, and (j) the temperature T_I of pickup protons. The white line in the T_S plot (d) depicts the projection of the *Voyager 2* trajectory on the meridional plane.
(A color version of this figure is available in the online journal.)

Sample solution; 30° dipole, model computed in three Regions (1-20Rs; 20-45Rs; 45Rs-3AU)
Outer section 0.2AU to 3 AU visualized here
Selected variables shown:

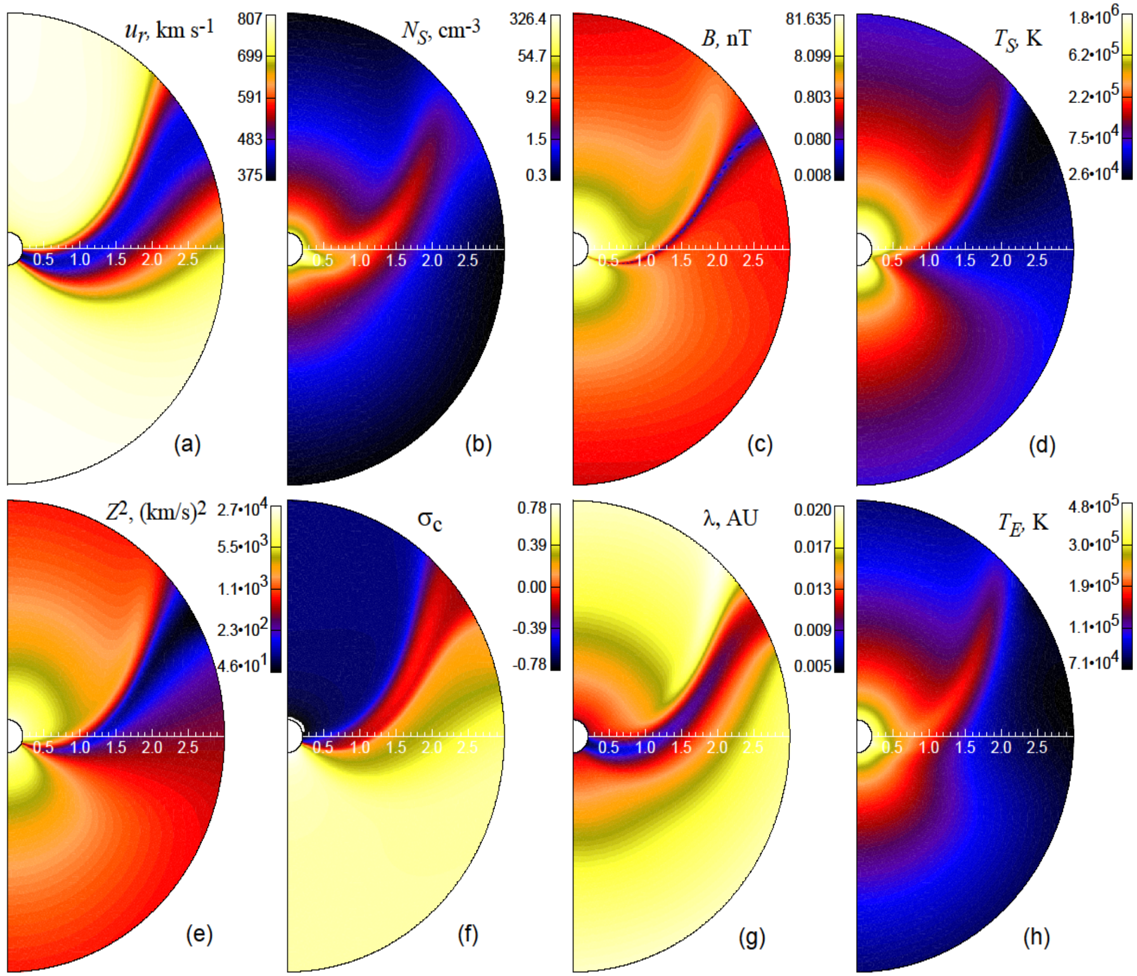

Global model compared to Ulysses data

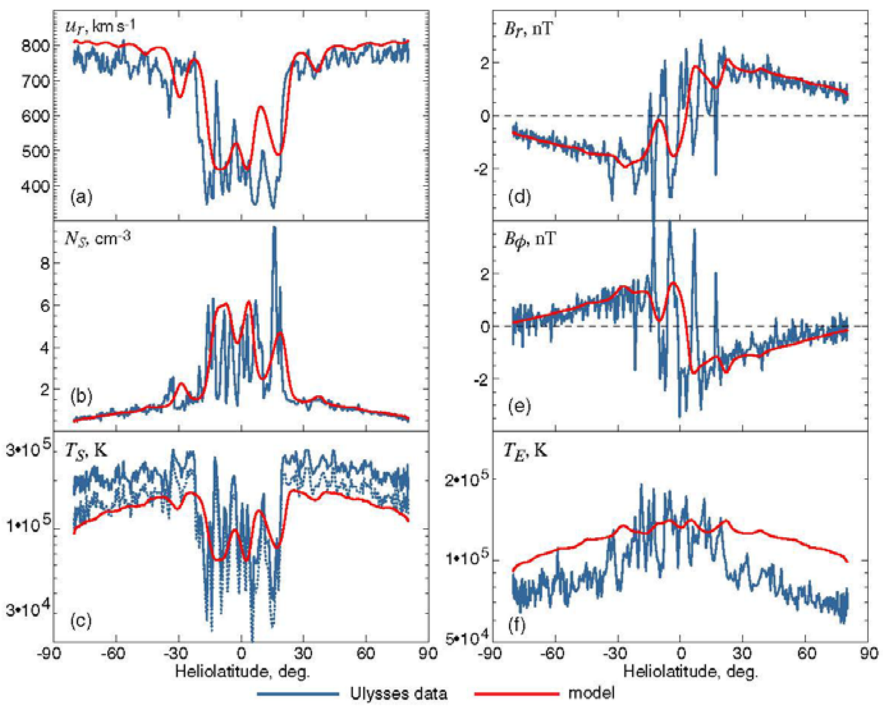

Figure 8. Simulated profiles (red) for a source magnetic dipole on the Sun tilted by 10° (with respect to the solar rotation axis) vs. *Ulysses* daily averages of plasma and magnetic field parameters measured during the first fast latitude transit of *Ulysses* in 1994–1995. The parameters shown are: the radial velocity u_r (a), the number density of solar protons N_S (b) and their temperature T_S (c), the radial B_r (d) and azimuthal B_ϕ (e) magnetic field, and the electron temperature T_E (f). Two estimates, "T-large" and "T-small" of the proton temperature measured by *Ulysses* are shown by blue solid and dotted lines, respectively.

(A color version of this figure is available in the online journal.)

Global model: effect of improved turbulence models (eddy resistivity & eddy viscosity) 0.3-10 AU

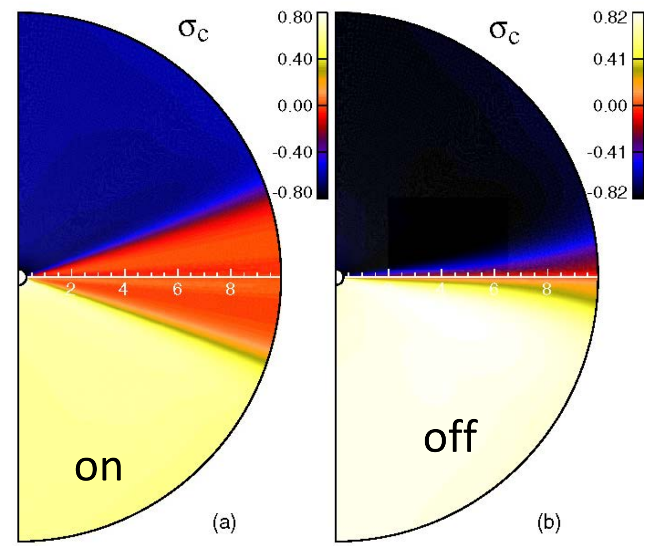

Usmanov et al, ApJ, 2014

Global simulation with dipole tilt and turbulence modeling

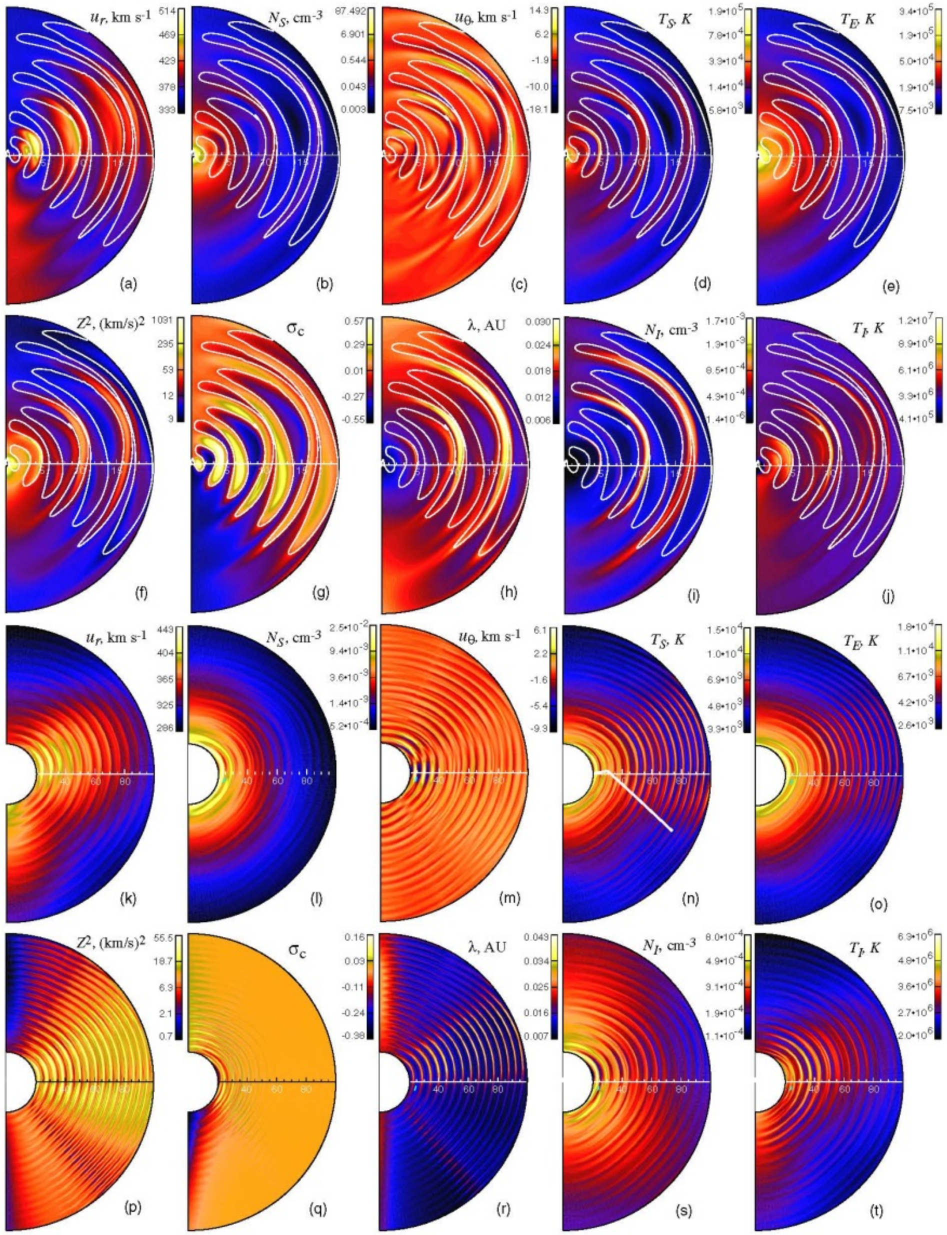

Figure 11. Contour plots in the meridional plane $\phi = 0°.75$ from 0.3 to 20 AU (a–j) and from 20 to 100 AU (k–t) of the mean-flow and turbulence parameters for Carrington Rotation 2123. The white lines in (a–j) depict the heliospheric neutral sheet ($B_r = 0$). The white line in the plot (n) shows the projection of the *Voyager 2* trajectory on the meridional plane.

THE GOAL:
Multi-scale Modeling of Turbulence in Global Simulation with sub-grid MHD and sub-grid kinetic modules

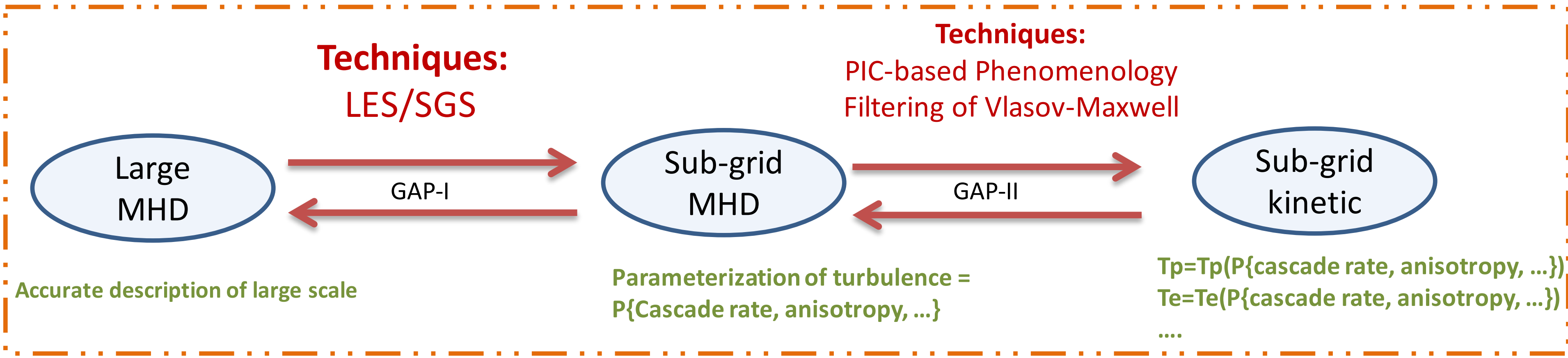

Cutting edge questions: can

structure formation
intermittency
phenomenology of kinetic physics

be built into turbulence modeling??

A topic of ongoing and future work…

These effects are going to be difficult!

See Miesch et a, SSR 2015

Some types of intermittency and potential effects on solar prediction

(1) Large scale/low frequency intermittency
   - variability of sources
   - Inverse cascade (space) ←→ 1/f noise (time)
   - Effects of dynamics on the "slow manifold"
   - → Dynamo reversals, rare events (big flares?)

(2) Inertial range intermittency
   - "scaling" range
   - reflects loss of self similarity at smaller scales
   - KRSH
   - → This is a lot of what you see and measure

(1) Dissipation rage intermittency
   - vortex or current sheets or other dissipation structures
   - usually breaks self similarity because there are characteristic physical scales
   - → Controls local reconnection rates and local dissipation/heating;
     small scale "events"

Inner boundary conditions

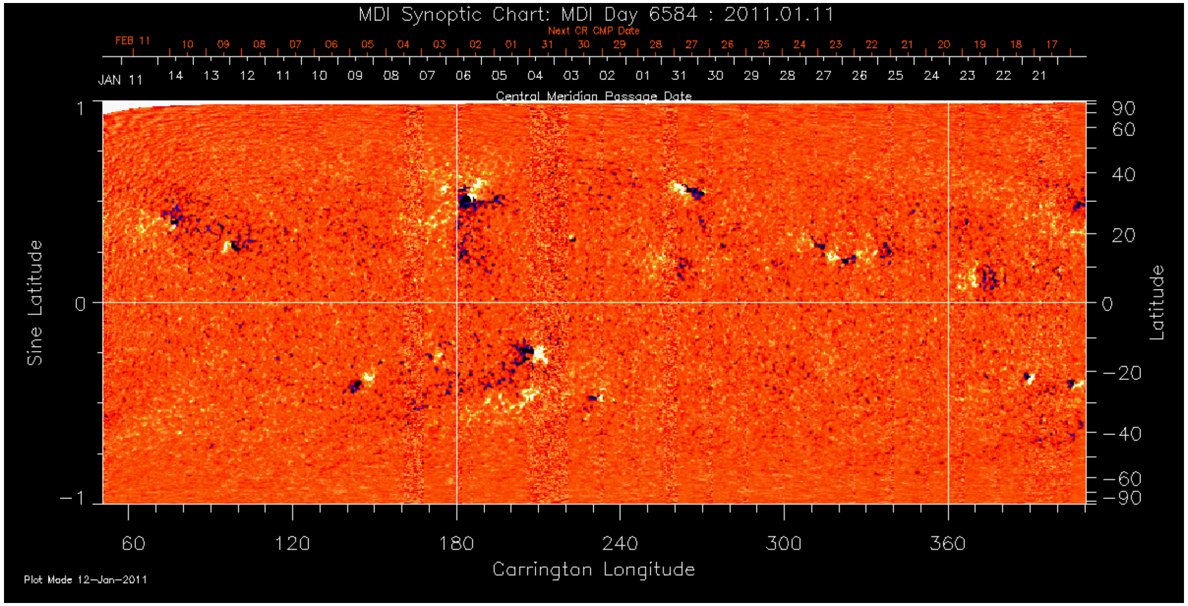

Largest scale structures

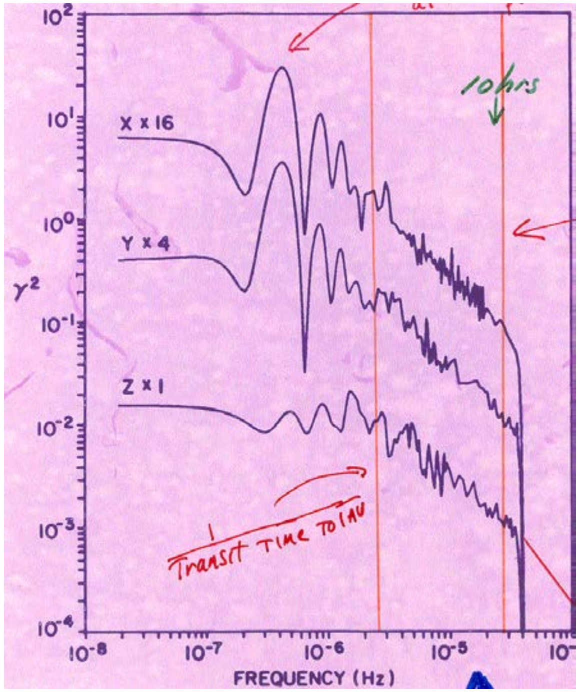

1/f noise:

orgin & implications for prediction

Very low frequency/very large scale intermittency

- 1/f noise:
  - Gives “unstable” statistics – bursts and level-changes
  - Long time tails on time correlations
  - Generic mechanisms for its production (Montroll & Schlesinger, 1980)
  - Often connected with inverse cascade, quasi-invariants,
  - highly nonlocal interactions (opposite of Kolmogorov’s assumption!)

- Dynamo generates 1/f noise (experiments: Ponty et al, 2004
    - connected to statistics of reversals (Dmitruk et al, 2014)
  - 1/k → 1/f inferred from LOS photospheric magnetic field
  - 1/f signature in lower corona
  - 1/f signatures observed in density and magnetic field in solar wind

  at 1 AU (M+G, 1986; Ruzmaiken, 1988; Matthaeus et al, 2007; Bemporad et al, 2008)

An example from 3D MHD with strong mean magnetic field

(Dmitruk & WHM, 2007)

- nearly in condensed state
- energy shifts at times scales of 100s to 1000s Tnl
- characteristic Tnl ~ 1
- Where do these timescales come from ?

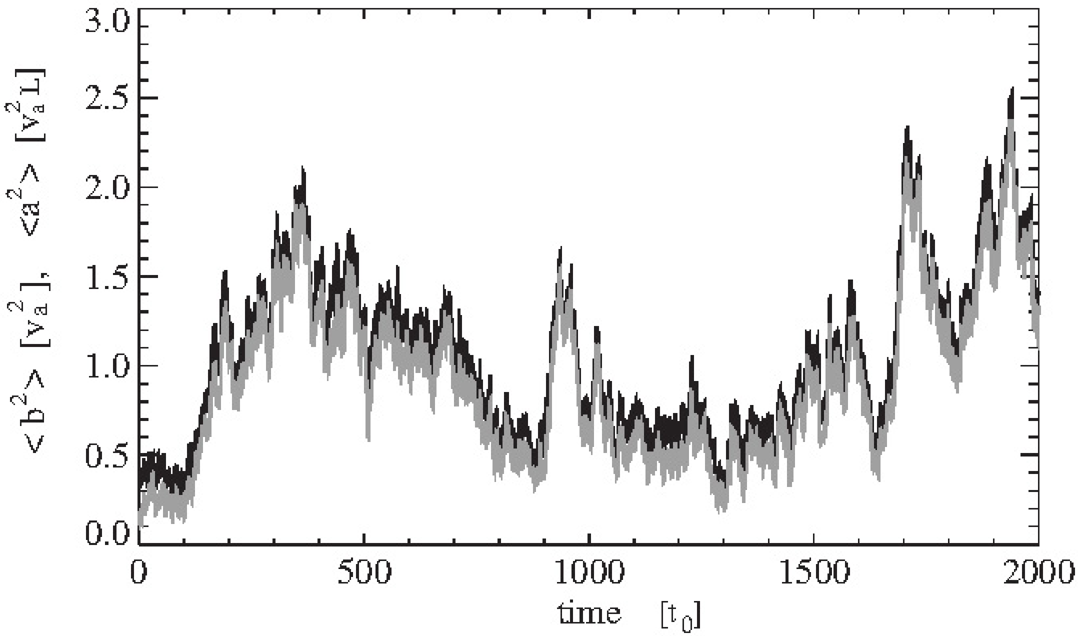

Numerical experiments on MHD Turbulence with mean field: onset of 1/f noise due to “quasi-invariant”

behavior of
a Fourier mode
In time, from
simulation

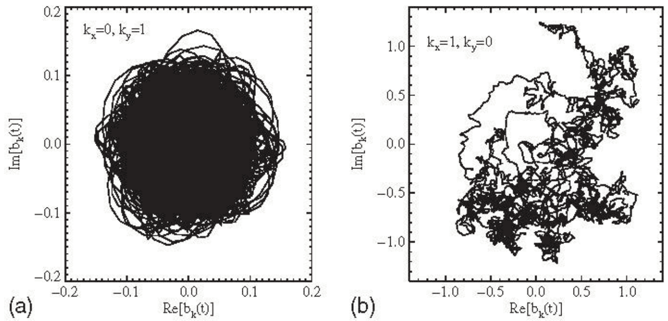

Eulerian frequency
spectrum:
transform of
one point
two time
Correlation fn.

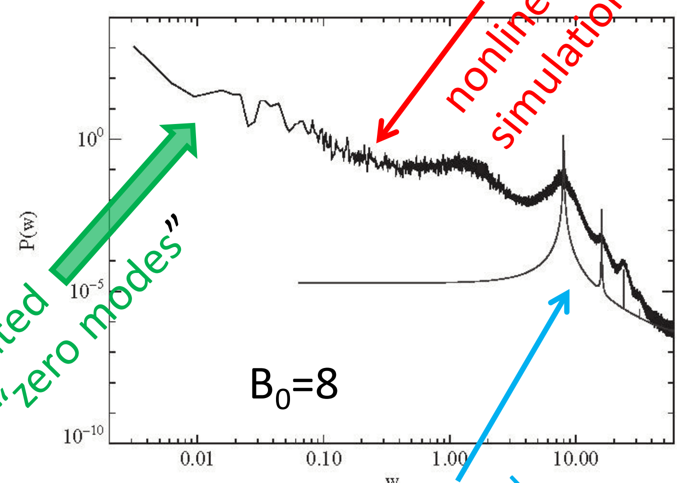

Eulerian frequency spectra

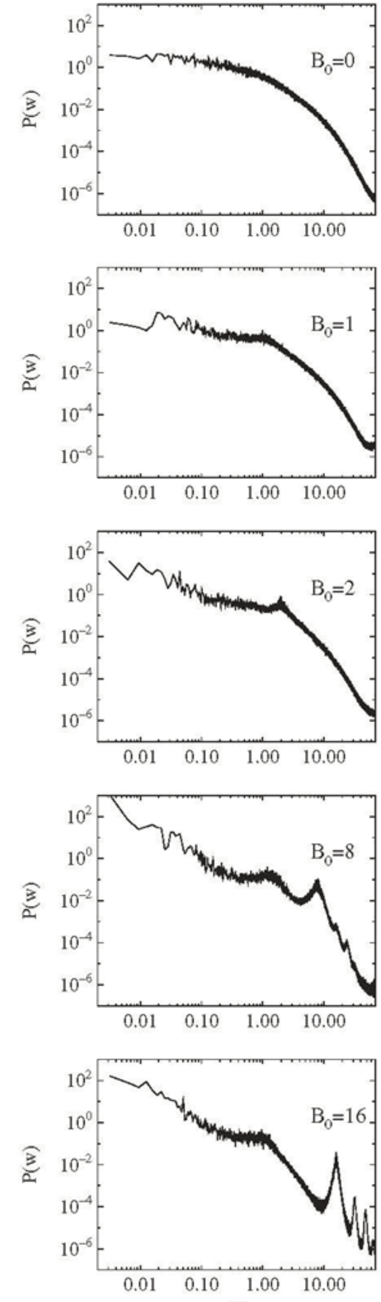

Increasing B_0

Dmitruk & Matthaeus, 2009

1/f: 1AU, MDI and UVCS – high/low latitude comparisons

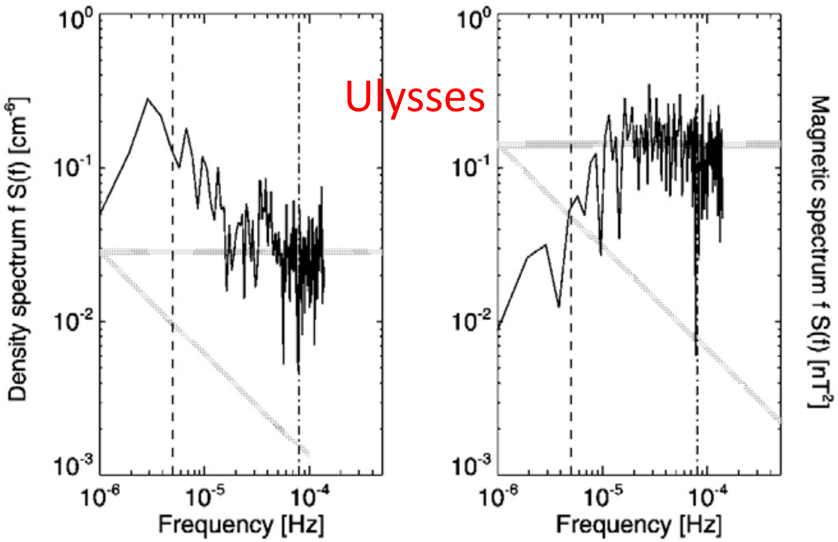

FIG. 1.—Examples of compensated spectra, $fS(f)$, showing intervals of $1/f$ noise, in magnetic field (*right*) and density (*left*) , from *Ulysses* data at low latitude, near 43° latitude, for days 116–176, 1996. Vertical dashed lines indicate the approximate frequency range of $1/f$ noise reported by Matthaeus & Goldstein (1986). Shaded bars suggest $fS(f) \sim f \times 1/f$ variation (flat), and, for reference, $fS(f) \sim f \times 1/f^{5/3}$ "Kolmogoroff" variation.

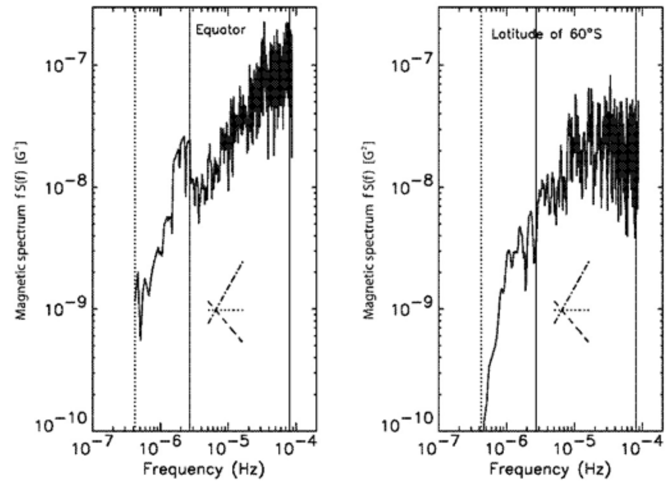

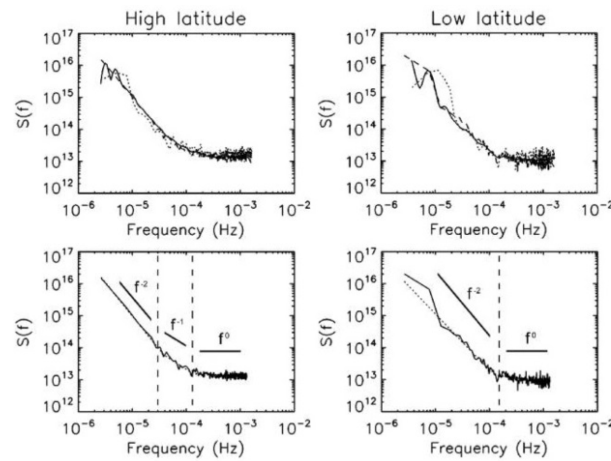

FIG. 3.—*Top*: Lyα power spectra $S(f)$ (photons^2 cm^{-4} s^{-2} sr^{-2}) from FT (*dotted lines*), WT (*solid lines*), and LS (*dashed lines*) analyses averaged over a 10° latitude interval around the south pole (*left*) and around a latitude of 60° southeast (*right*) in order to show latitudinal differences in the spectral range extents of $1/f$ interval (see text). *Bottom*: Lyα power spectra from LS analysis (*solid lines*) averaged over the same latitude intervals as in the top panels and the corresponding fitting functions (*dotted lines*); reference solid lines show the f^{-2}, f^{-1}, and f^0 slopes.

Matthaeus et al, ApJ 2007
Bemporad et al, ApJ 2008

1/f noise and reversals in spherical MHD dynamo

Incompressible MHD spherical Galerkin model low order truncation

→ Run for 1000s of Tnl
→ See ramdon reversals of the dipole moment
→ 1/f noise with rotation and or magnetic helicity

Dmitruk et al, PRE 2014

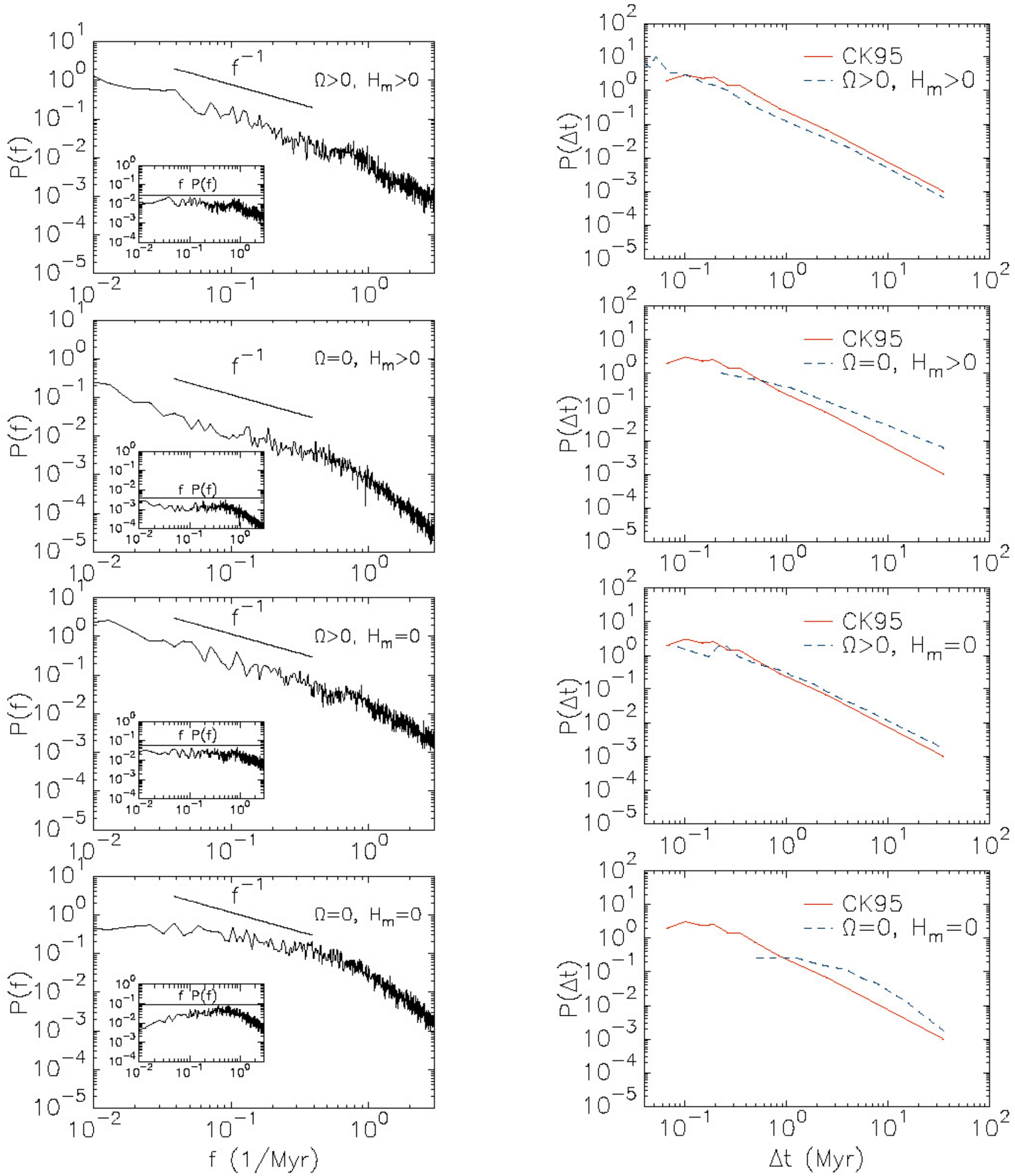

With rotation/helicity → Waiting times for reversals scale like geophysical data!

Heliospheric effects associated with flux tube structure/boundaries/coherent structures/current sheets

- Heating: proton Temp elevated at & near coherent magnetic structures
  → enhanced dissipation & kinetic activity

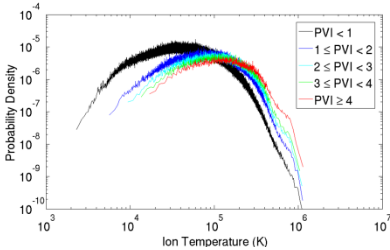

Osman et al, ApJ 2011)

- Dropouts: sudden, energy- dependent changes in observed SEP flux
  → field lines & particles temporarily trapped in in flux tubes, bounded by coherent magnetic structures

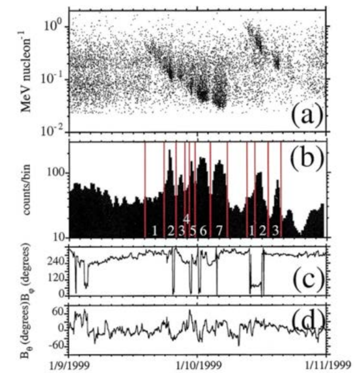

Mazur et al, 2000
See also
Ruffolo et al, 2003;
Tooprakai et al, 2007;
Seripienlert et a, 2011
Kittinaradorn et al, ApJ 2009

- Moss chromospheric brightness pattern
  → energize particles by nanoflares in corona; connectivity down to chromosphere structured by flux tubes

Kittinaradorn et al, ApJ 2009

- SEPs: enhanced fluxes of suprathermal particles at & near observed coherent structures in SW
  → transport? reacceleration?

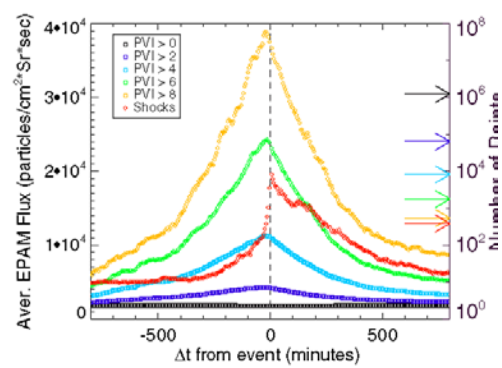

Tessein et al, ApJ, 2013

Strength of electric current density in shear-driven kinetic plasma (PIC) simulation (see Karimabadi et al, PoP 2013)

Thinnest sheets seen are comparable to electron inertial length. Sheets are clustered
At about the ion inertial length → heirarchy of coherent, dissipative structures at kinetic scales

Issues relating to reconnection, plasmoids and topology

Multiple islands in RZ: secondary islands form at convective timescales

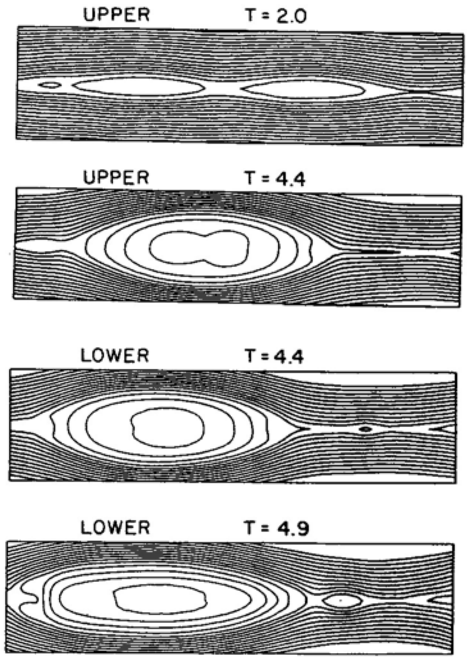

FIG. 5. Closeup contours of magnetic field lines showing bubbles for the $\mu^{-1} = 1000$ run. Small bubbles appear at the far left of the upper current sheet region at $t = 2.0$ and at $t = 4.4$. A small bubble has appeared along the lower sheet at 4.4 and has grown by $t = 4.9$.

IV. DISCUSSION: TURBULENT RECONNECTION

The magnetic irregularities formed in the reconnection zone because of electric field fluctuations change the field topology and form multiple X points. The nonsteadiness of

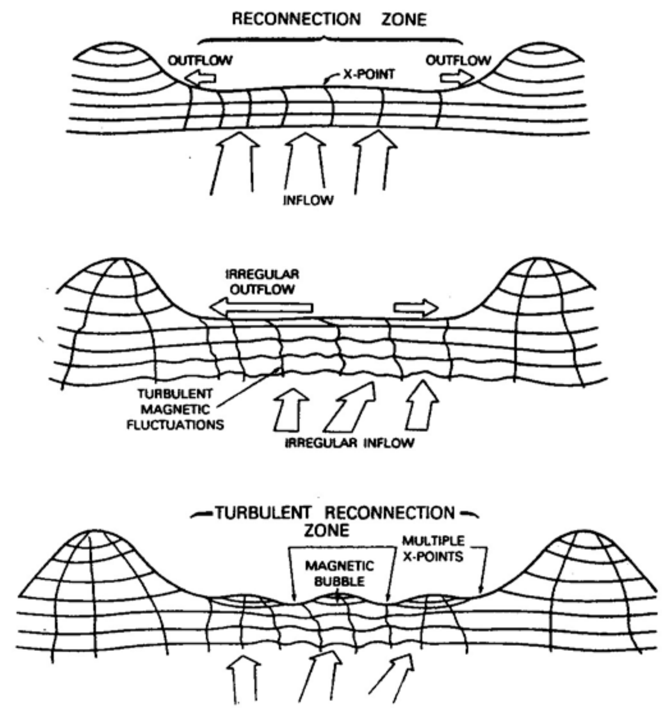

FIG. 6. Sketches of the surface of vector potential in the area around the reconnection zone, suggesting the effects of turbulence. (a) A smooth reconnection zone. The central X point is a saddle point of vector potential—a steep maximum across the neutral sheet and a shallow minimum along it. (b) Adding fluctuations produces irregularities in the surface, which are transported towards the reconnection zone by the nonsteady flow pattern. (c) The topology of the magnetic field is modified in complicated ways by the turbulence. Reconnection proceeds rapidly because of multiple X points and magnetic bubbles in the reconnection zone.

Reynolds number effect expected!

See also: Alfvenic "plasmoid instability",
and Richtmeyer-Meshkov instability of shocks

Matthaeus & Lamkin, PoF, 1985

Profileration of Xpoints in MHD: spatial picture and space-time evolution

- A small region of a 16Kx16K Fourier spectral simulation with threefold oversampling of Kolmogorov scale, analyzed on 32Kx32K grid; Rm = 50000, total of 5649 X-points at peak time

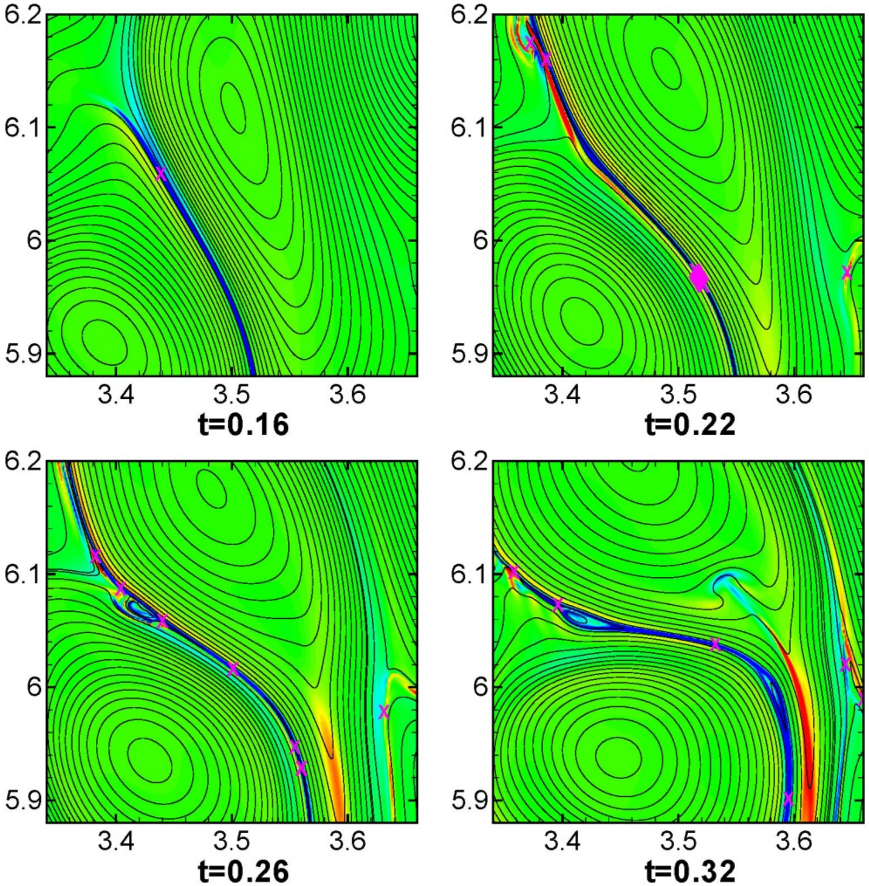

Magnetic field lines, electric current density, and X points

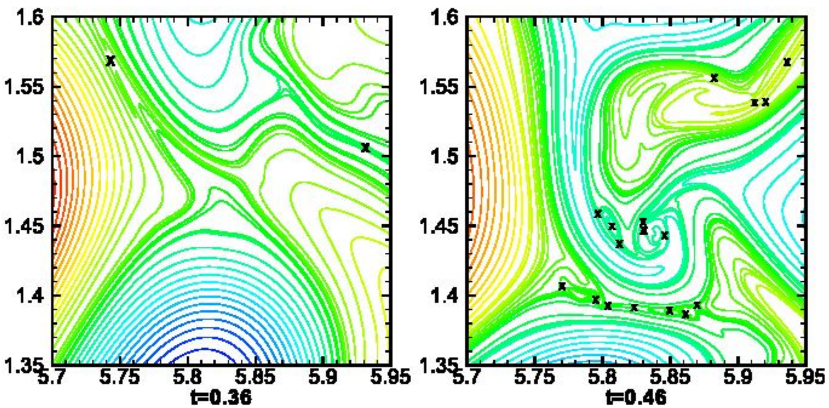

Another region
at two times

Wan et al, PoP, 2013

Plasmoid scaling properties in **2D** MHD

Examine many runs at varying resolution, initial data and Reynolds numbers

Wan et al, PoP, 2013

- Number of Xpoints/flux tubes
  - Vs Rm (at peak dissipation)

    Can be understood in terms of basic cascade physics

  - vs time

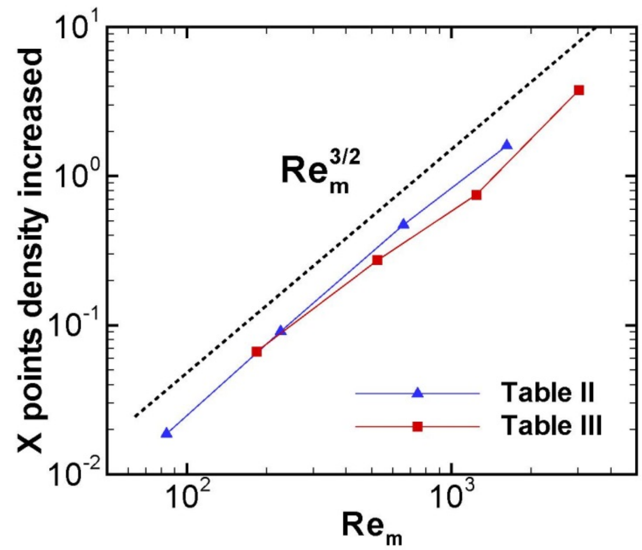

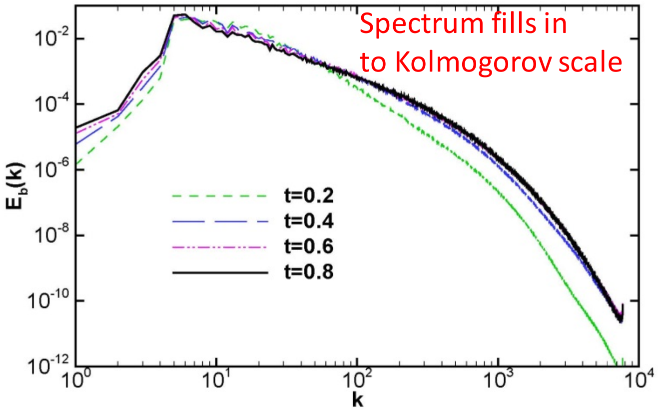

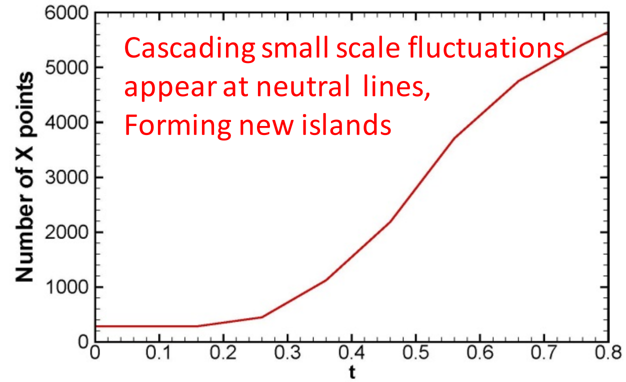

- Resolution 16384^2
- Rm=50000
- Kmax/Kdiss = 3.4

Many reconnection sites form in ***shear-driven kinetic plasma*** with initially uniform magnetic field

(Top) whole field; (Bottom) zoom of two sub-regions.

Total of 278 X-points identified;

Red circles (6) strongest reconnection sites (> 0.1 in Alfven unit)

Pink diamonds (66) strong reconnection rates (0.05 to 0.1 in Alfven unit),

Grey boxes (63) moderate reconnection sites (0.025 to 0.05 in Alfven unit),

Black "X" (143) other weaker sites.

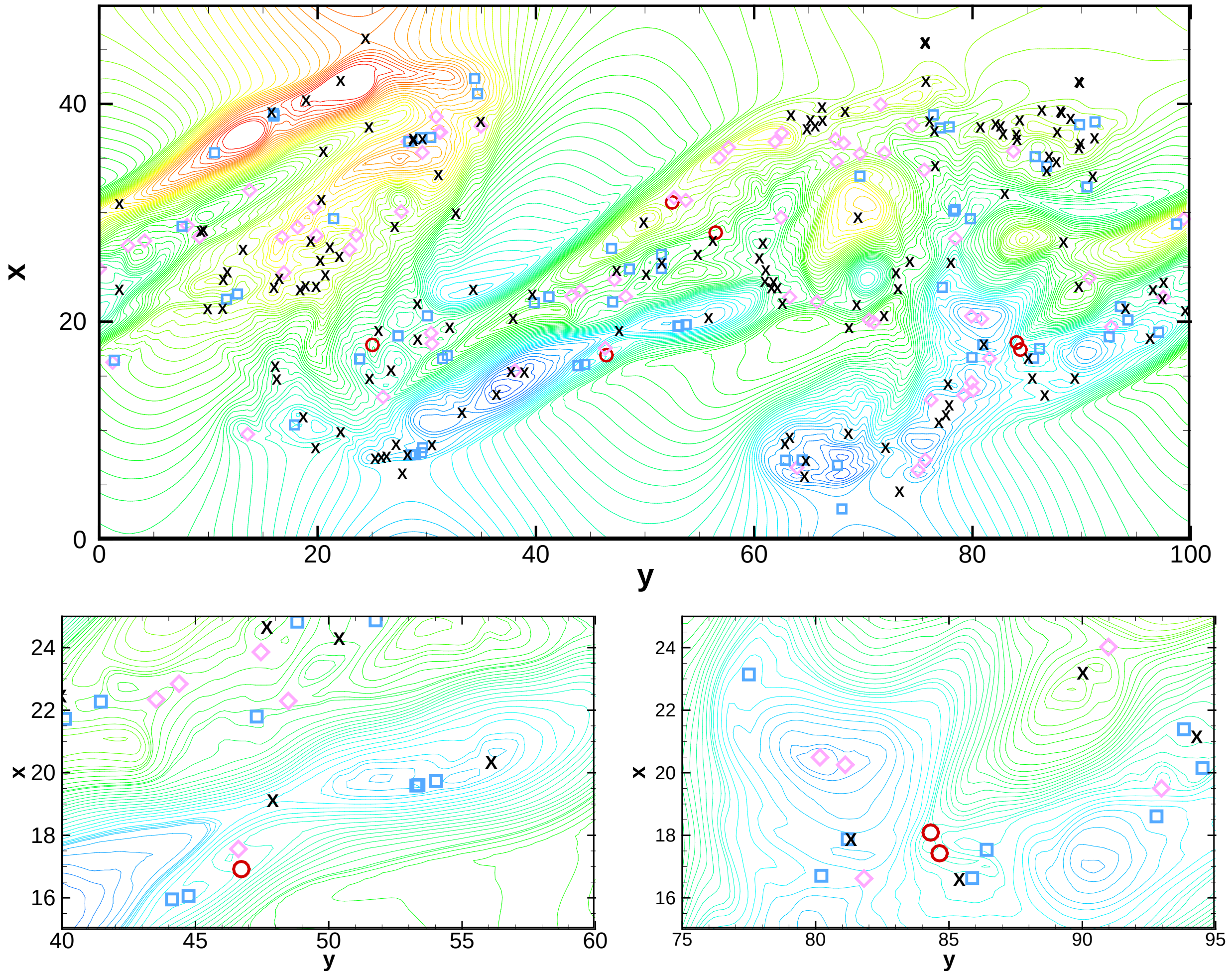

Karimabadi, Roytershteyn, Wan et al

Reconnection in **3D**

- Very complex structures are possible

3D Hall MHD: two examples (Dmitruk & Matthaeus (2006)

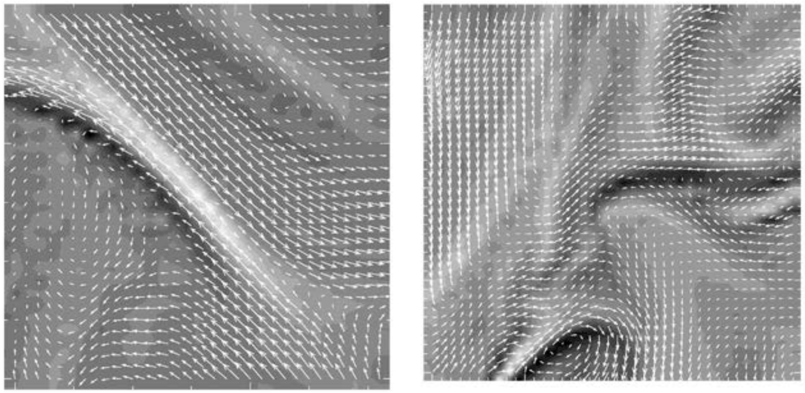

Priest & Pontin, PoP 2009

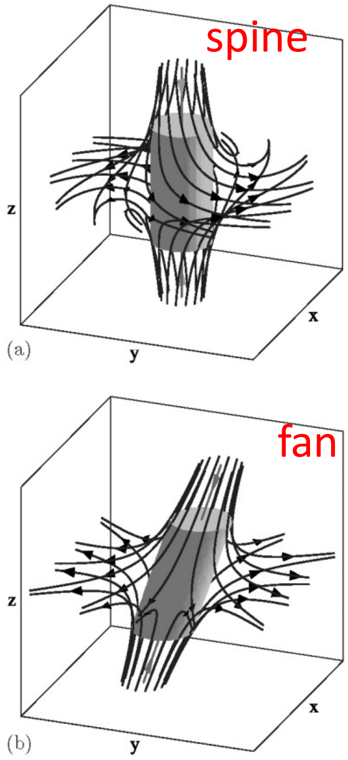

- Weakly 3D Reduced MHD affords a useful direction

  - Slowly varying in z-direction
  - “nanoflare” problem
  - Driven by low-frequency boundary motions, appropriate for solar flux tubes driven by low-frequency photospheric stirring of the magnetic footpoints (Parker 1972; Einaudi et al. 1996, Rappazzo & Velli 2010).

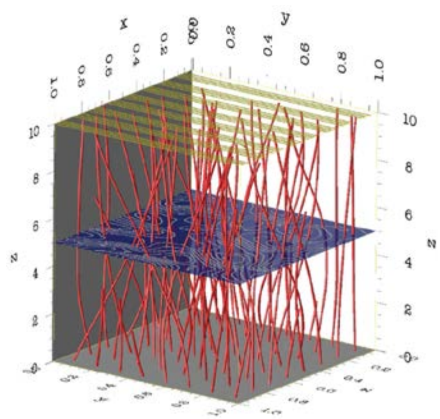

View of currents in boundary driven weakly 3D Reduced MHD

Wan et al, ApJ 2014

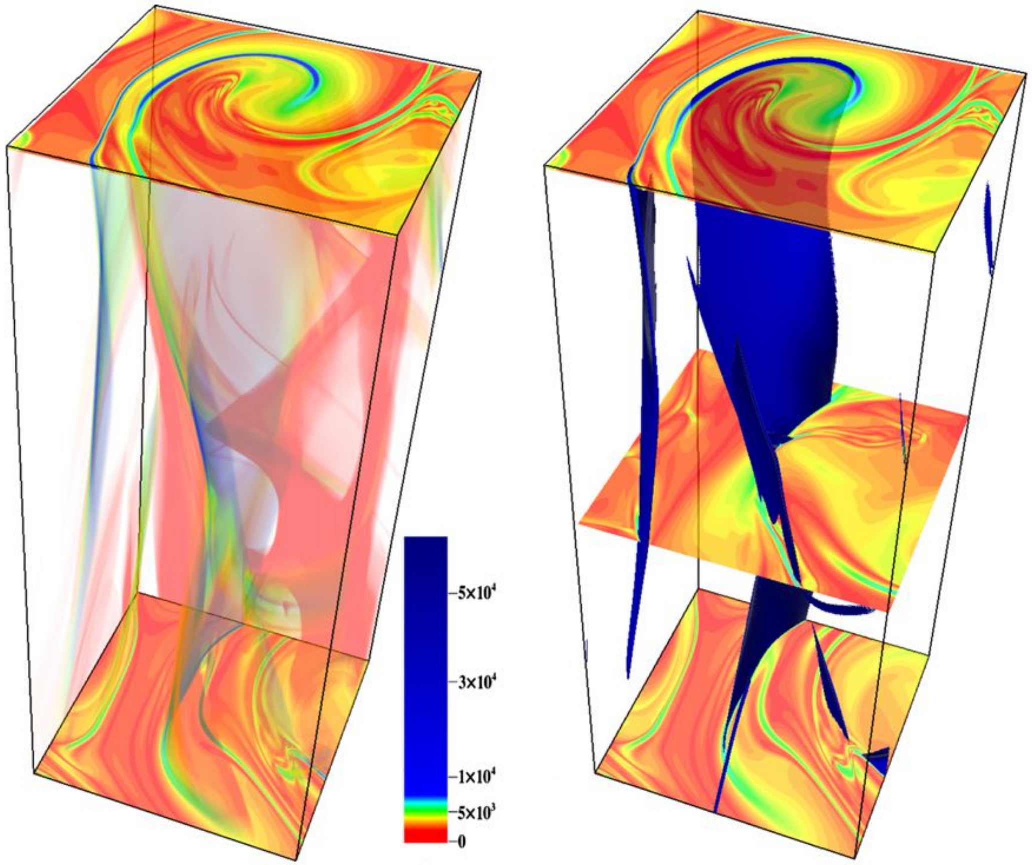

Figure 1. Two renderings of the 3D electric current density at $t \sim 30\tau_A$, when the simulation has attained a statistically steady state. Left: 3D translucent shading of the current density. Right: iso-surfaces of electric current density at a near-peak value. In both plots color contours of the current density are shown in selected cross sectional 2D planes. The legend indicates corresponding numerical values. Only 1/16 of the simulation box $(0.25 \times 0.25 \times 10)$ is shown.

X-point-current peak distances & *LOCAL* reconnection rates

Wan et al, ApJ 2014
See also Zhdankin et al, 2013

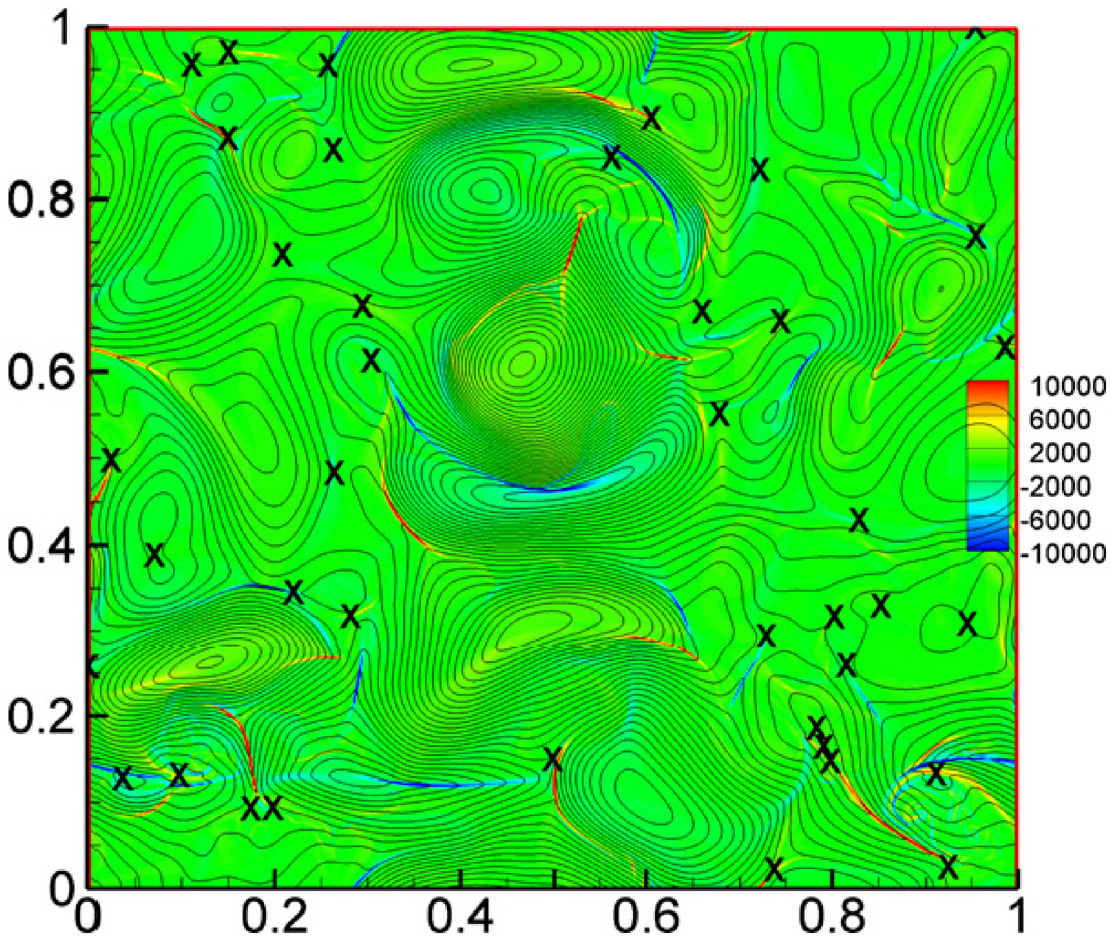

Distribution of distance from Xpoint-to- nearest current sheet

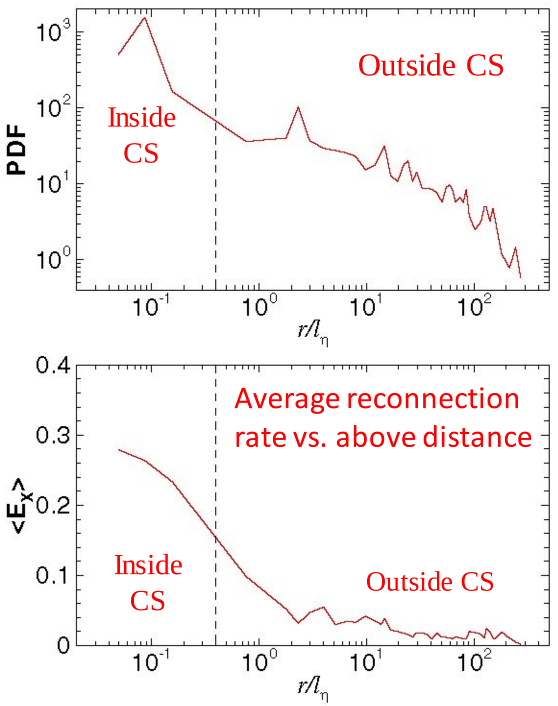

Figure 12. Top: PDF of the distance (r) from X-points to the closest current sheet (region with $|j| \gtrsim 6\, j_{\rm rms}$), normalized by the Kolmogorov dissipation scale ℓ_η. Bottom: conditional average of electric field at the X-points, conditioned on the distance from the X-point to the closest current sheet. Grid length, Δx, is indicated in both panels by vertical dashed lines.

Separation of Xpoints and current sheets is an important reason for bursty/nonsteady reconnection in 3D! Need to define reconnection locally!

Test particles in RMHD

Ambrosiano etal,JGR1988
Dmitruk et al, 2003, 2004
Chandran et al, ApJ 2010
Rappazzo et al, ApJ 2008, 201
Dalena et al, 2013

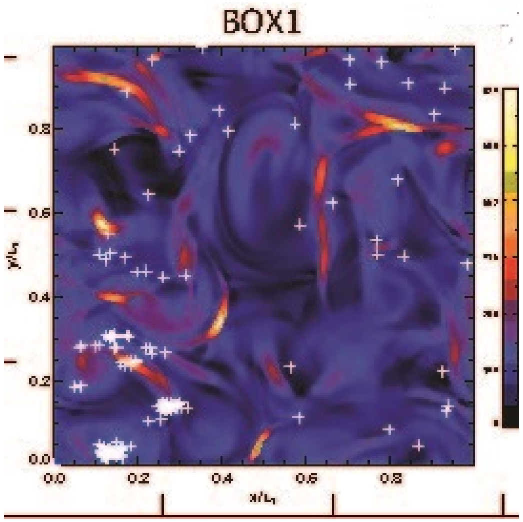

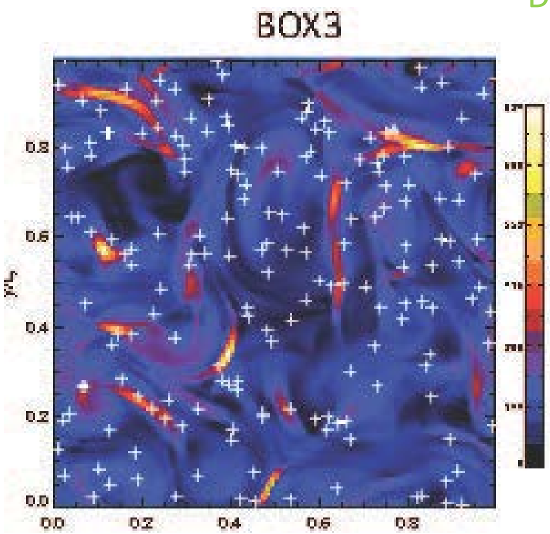

Stage 1 – parallel acceleration dominates, highly associated with current sheets

Stage 2, larger gyroradii, perpendicular acceleration dominates;
resonant (as in betatron);
associated with electric field inhomogenities,
and therefore more loosely with current structures

Coupling of structures to particles

Particles are energized anisotropically!

3D MHD/test particles with strong B_0: distributions at short times < crossing time of Lc

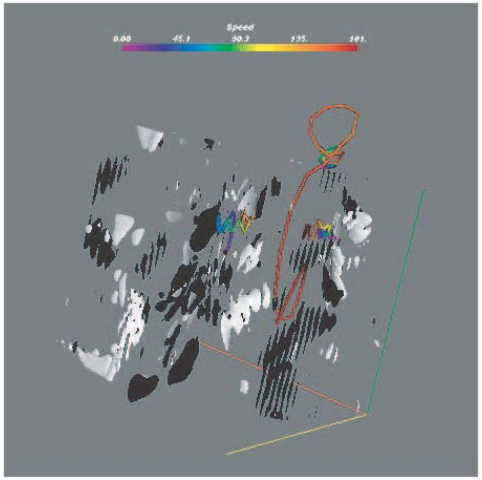

protons

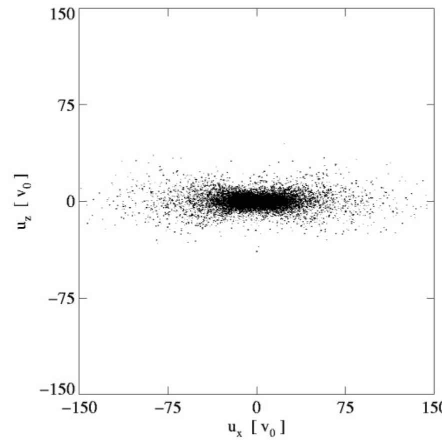

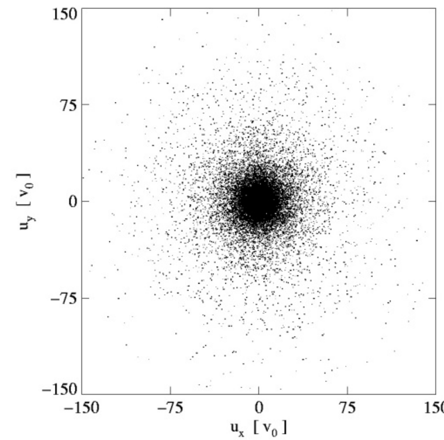

B_0 direction

perp plane

Trajectories and current structures

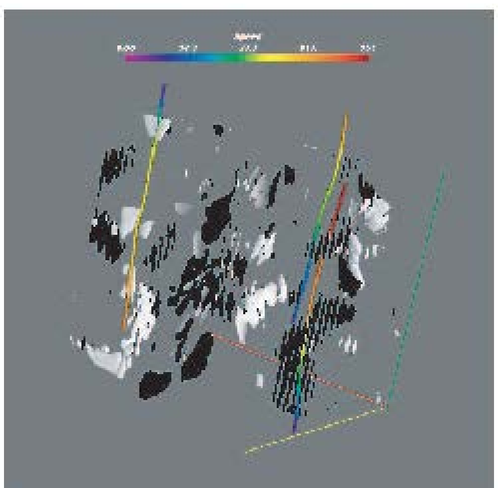

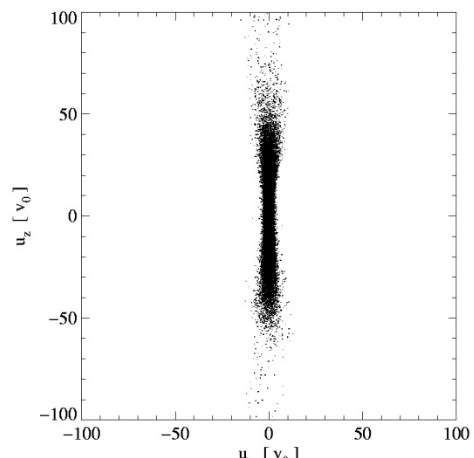

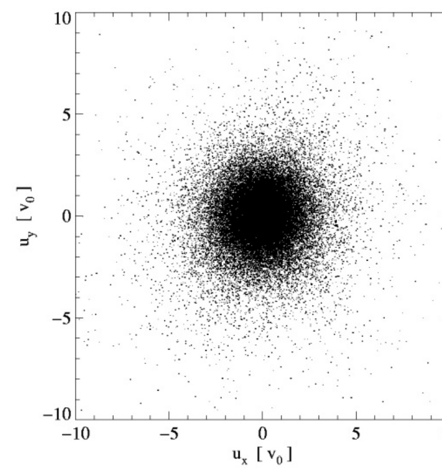

electrons

Dmitruk et al, 2004

Partitioning of heating between protons and electrons

- varying turbulence level Z^2
- constant initial plasma beta

Average proton & electron heat functions

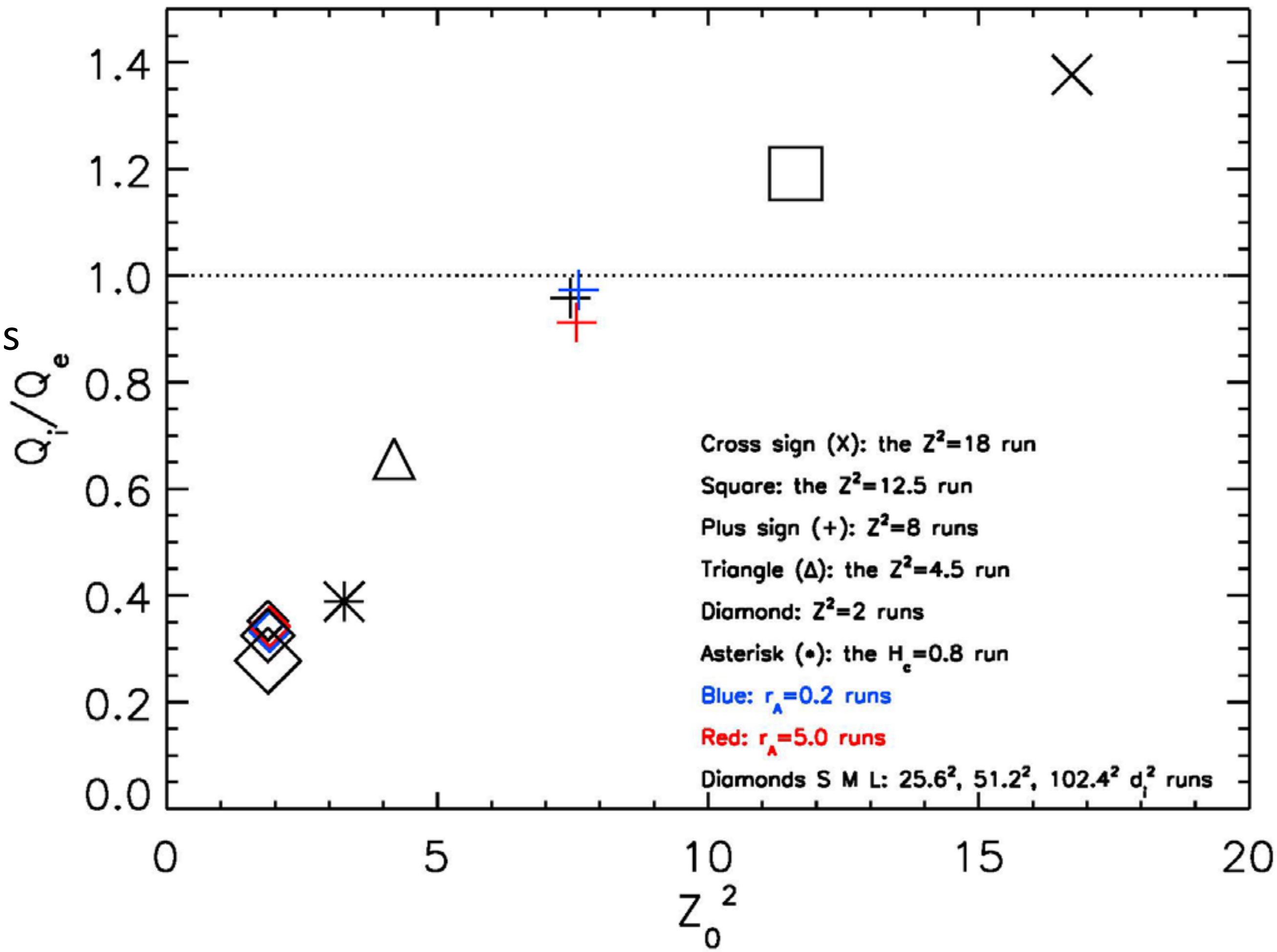

Wu et al, PRL, 2013

Cascade rate, turbulence strength & proton/electron heating

Evidently, protons absorb a larger fraction of the cascaded energy when the turbulence is stronger

Dmitruk et al, 2004
Smith et al, ApJL, 2006
Matthaeus et al, ApJ, 2008
Chandran et al, ApJ, 2010
Osman et al, ApJL, 2011
Wu et al, PRL, 2013

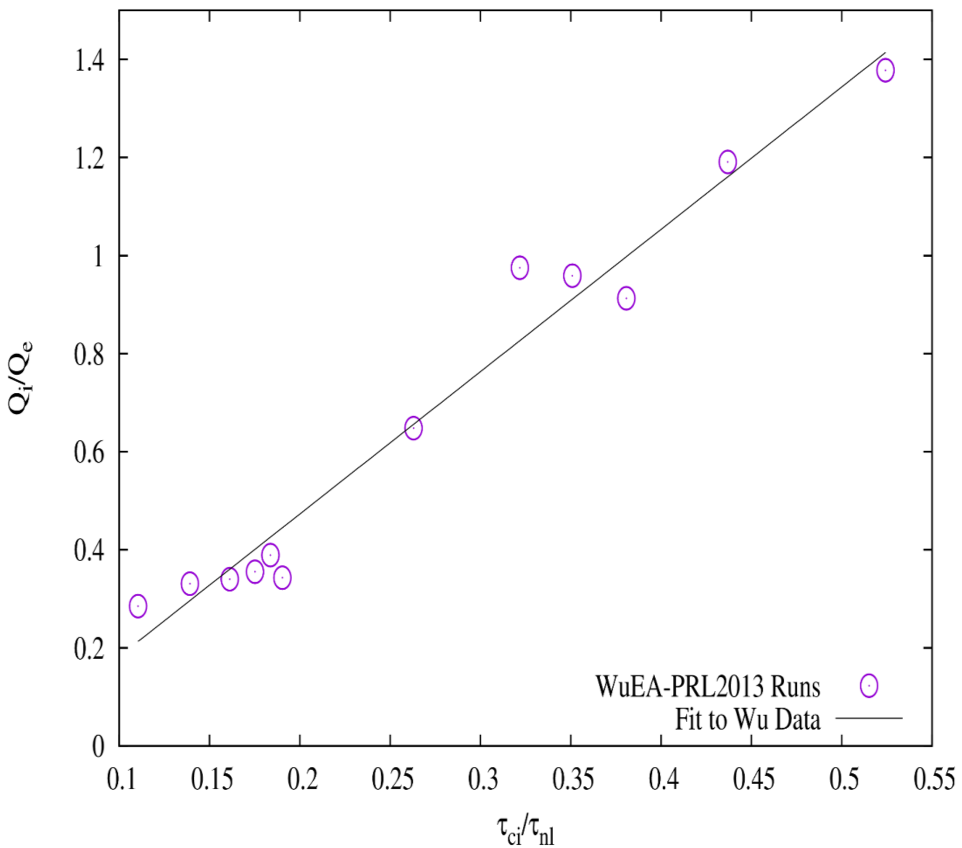

Ratio of proton gyroperiod to nonlinear cascade time

Parashar et al, 2015;
Adapted from Wu et al, PRL, 2013

Protons hotter in fast solar wind

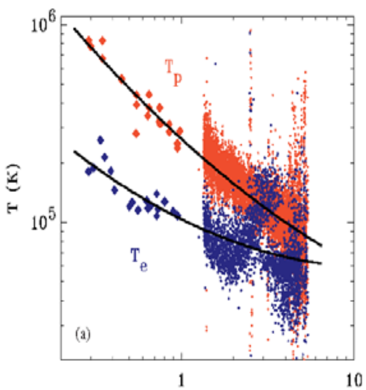

Cranmer et al, ApJ, 2009

3D PIC turbulence

- Dissipation is intermittent in 3D collisionless plasma

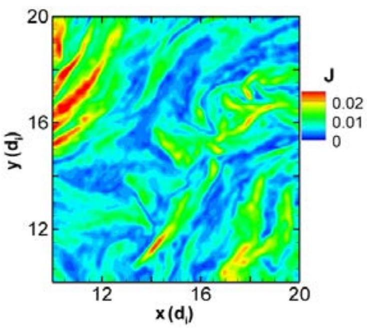

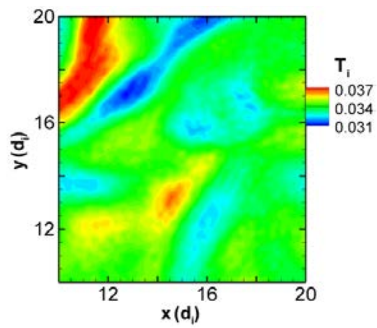

Map of j.E

Map of Tp in same plane

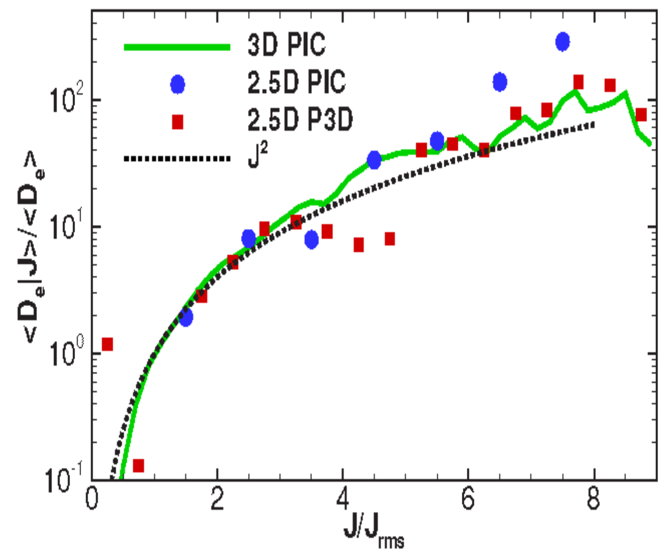

FIG. 6: Conditional average of dissipation D_e calculated conditioning on the value of current density, normalized by the global average dissipation rate $< D_e >$. Also shown are the same results from two different 2.5D PIC simulations [10] and MHD simulations.

Average De binned by |J|

- Increases with |J|
- About the same in 2D & 3D

Almost same scaling with current density as in MHD!!!

3D PIC

Wan et al, PRL, 2015
Roytershteyn et al, 2015

2048^3 spatial resolution; 1.7 trillion particles

Coherent structures in electric current density

3D+3v hybrid-Vlasov

Servidio, Valentini et al, JPP 2014

128^3 real space x 51^3 v-space

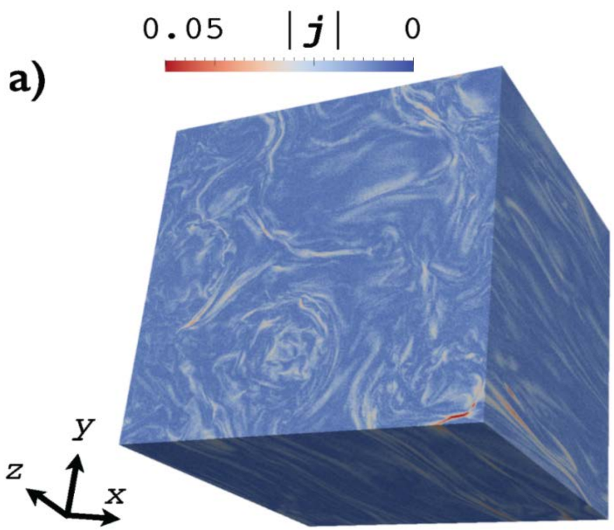

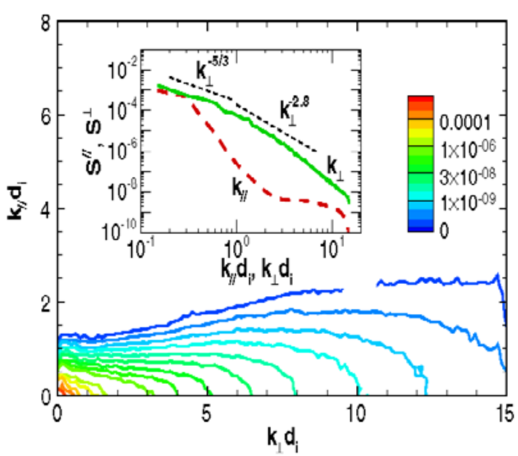

26 *S. Servidio et al.*

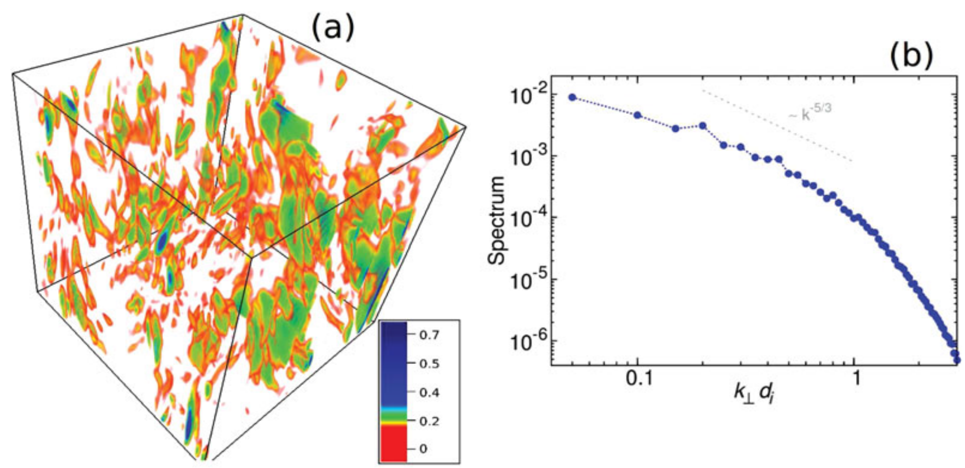

FIGURE 18. (Colour online) (a) 3D shaded contour of the current density $|\boldsymbol{j}|$ for a six-dimensional HVM simulation. As for fluid models, strong current sheets characterize the turbulent pattern. (b) Reduced spectrum of the total magnetic field as a function of $k_\perp d_i$. The dashed (gray) line represents a reference for the eye, indicating the Kolmogorov prediction of turbulence. The case reported is for $\beta = 0.5$ and $\delta b/B_0 = 1/3$.

Summary: Kinetic plasma turbulence

- Kinetic cascade
- Waves vs turbulence
- Heating processes
- intermittency

- Active area of study to develop a phenomenology needed to improve cross scale modeling

Summary: pathway to cross scale modeling

Self-consistent MHD Improvements

- MHD subgrid stresses
- Eddy diffusivities
- Spatial diffusion
- Alpha effect
- Production terms
- Heat conduction….Etc…

Mesoscale (MHD) Model

Cross Scale Kinetic Improvements

- Kinetic subgrid stress
- Heating, Te and Tp
- Anisotropies
- Suprathermals, Etc…

Microscale (kinetic) Model

Turbulent Transport

- Turbulence distribution in the heliosphere
- Connection between local turbulence & kinetic signatures

1D + Heating & Acceleration in Coronal Holes

- Quantitative physics based coronal heating model
- Critical evaluation of turbulence driven fast wind models

3D Solar Wind Model

- Self consistent coupling of large scales and turbulence
- Extension to kinetic effects enables numerous observational connections

3D Corona

- 3D data driven model w/ consistent turbulence & kinetics
- Tool for Solar Probe & Solar Orbiter

Space Sci Rev
DOI 10.1007/s11214-015-0190-7

Large-Eddy Simulations of Magnetohydrodynamic Turbulence in Heliophysics and Astrophysics

Mark Miesch[1] · William Matthaeus[2] · Axel Brandenburg[3] · Arakel Petrosyan[4,5] · Annick Pouquet[6,7] · Claude Cambon[8] · Frank Jenko[9] · Dmitri Uzdensky[10] · James Stone[11] · Steve Tobias[12] · Juri Toomre[13] · Marco Velli[14]

Received: 15 April 2015 / Accepted: 17 July 2015

Abstract We live in an age in which high-performance computing is transforming the way we do science. Previously intractable problems are now becoming accessible by means of increasingly realistic numerical simulations. One of the most enduring and most challenging of these problems is turbulence. Yet, despite these advances, the extreme parameter regimes encountered in space physics and astrophysics (as in atmospheric and oceanic physics) still preclude direct numerical simulation. Numerical models must take a Large Eddy Simulation

✉ M. Miesch
miesch@ucar.edu

W. Matthaeus
whm@udel.edu

A. Brandenburg
brandenb@nordita.org

A. Petrosyan
a.petrosy@iki.rssi.ru

A. Pouquet
pouquet@ucar.edu

C. Cambon
claude.cambon@ec-lyon.fr

F. Jenko
jenko@physics.ucla.edu

D. Uzdensky
Uzdensky@colorado.edu

J. Stone
jstone@astro.princeton.edu

J. Toomre
jtoomre@lcd.colorado.edu

M. Velli
mvelli@jpl.nasa.gov

1 HAO/NCAR, 3080 Center Green Dr., Boulder, CO 80301, USA

2 Dept. of Physics and Astronomy, University of Delaware, Newark, DE 19716, USA

Published online: 31 July 2015 Springer

Miesch et al,
SSR 2015